We are IntechOpen, the world's leading publisher of Open Access books
Built by scientists, for scientists

6,900
Open access books available

185,000
International authors and editors

200M
Downloads

Our authors are among the

154
Countries delivered to

TOP 1%
most cited scientists

12.2%
Contributors from top 500 universities

WEB OF SCIENCE™

Selection of our books indexed in the Book Citation Index
in Web of Science™ Core Collection (BKCI)

Interested in publishing with us?
Contact book.department@intechopen.com

Numbers displayed above are based on latest data collected.
For more information visit www.intechopen.com

# Development and Present Status of Organic Superconductors

Gunzi Saito and Yukihiro Yoshida

Additional information is available at the end of the chapter

1. Introduction

Since the first observation of superconductivity by K. Ones with a critical temperature of superconductivity (T_c) of 4.2 K on mercury (1911), many researchers have persuaded such exciting system on organic materials with vain. Even metallic behavior was hardly seen on the organic materials. Little's theoretical proposal (1964) for high T_c superconductivity ($T_c >$ 1000 K) was based on a polymer system having both a conduction path and highly polarizable pendants, which mediate the formation of Cooper pairs in the conduction path by electron-exciton coupling [1]. There are at least two inorganic polymer superconductors without doping (graphite and diamond are superconductors by doping: see Section 5), poly(sulfur nitride) $(SN)_x$ (1975, $T_c \leq 3$ K) [2] and black phosphorus (1984, $T_c \sim 6$ K at 16 GPa and 10.7 K at 29 GPa) [3], with crystalline forms. However, so far no organic polymers have been confirmed to show superconductivity which is easily destroyed by a variety of disorder. Only crystalline polymers were reported to exhibit metallic behavior: a doped polyaniline by chemical oxidation of monomers [4] and MC_{60} (Scheme 1) having linearly polymerized $C_{60}^{\bullet-}$ with one-dimensional (M = Rb, Cs) or three-dimensional (M = K) metallic behavior [5].
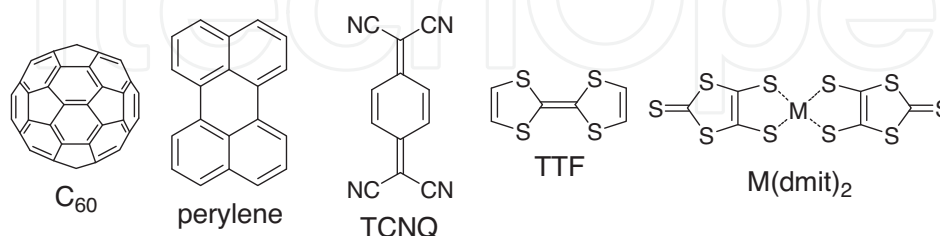
Scheme 1.

The Little's model accelerated the exploration of the conducting organic materials of low molecular weight, that had been started by the finding of highly conductive perylene•halides charge-transfer (CT) solids (10^0–10^{-3} S cm^{-1}) in early 1950s [6] and TCNQ

CT solids from the 1960s [7]. The first metallic CT solid TTF•TCNQ appeared in 1973 [8] based on the two main requirements for the conductivity, namely, (1) a uniform segregated stacking of the same kind of component molecules, and (2) the fractional CT state (uniform partial CT) of the molecules. Since TTF•TCNQ has a low-dimensional segregated stacking, it showed a metal-insulator (MI) transition (Peierls transition) below about 60 K. For TTF•TCNQ, the Peierls transition occurs by the nesting of the one-dimensional Fermi surface causing lattice distortion associated with the strong electron-phonon interaction and forms charge density wave (CDW). There are also several one-dimensional organic metals which show MI transitions by the formation of spin density wave (SDW) when the periodicity of the SDW coincides with the nesting vector of Fermi surface and no lattice distortion occurs in this case. An increase in the electronic dimensionality is inevitable to prevent the nesting of Fermi surfaces and develop superconductors. Several attempts have been made through "pressure", "heavy atom substitution", or "peripheral addition of alkylchalcogen groups" (Fig. 1). The latter two correspond to the enhancement of the self-assembling ability of the molecules.

Appropriate examples taking TTF derivatives are shown in Fig. 1. Based on TMTSF molecules several superconductors under pressure have been prepared with warped one-dimensional Fermi surface since 1980 (a in Fig. 1) [9–14]. In general, the ratio of transfer energies ($t_{//} / t_{\perp}$) is larger than 3 for one-dimensional Fermi surface and a closed two-dimensional Fermi surface is formed when $t_{//} \leq 3t_{\perp}$, where $t_{//}$ and $t_{\perp}$ are the transfer energies along the directions of the largest and second largest intermolecular interactions. The BO (BEDO-TTF) molecules afforded stable two-dimensional metals having two-dimensional Fermi surface (b in Fig. 1) owing to the strong self-assembling ability by intermolecular S···S and hydrogen-bonds [15], and only two superconductors are known since 1990 ($T_c \leq 1.5$ K). The substitution of an ethylenedioxy group with an ethylenedithio group (BO → ET (BEDT-TTF)) destabilized the metallic state of BO compounds and provided unstable two-dimensional conductors (c in Fig. 1). Consequently, variety of superconductors and other functional solids have been developed based on two-dimensional metals of ET since 1982 ($T_c \leq 13.4$ K) [16–20] and its analogues ($T_c \leq 10$ K) [21].
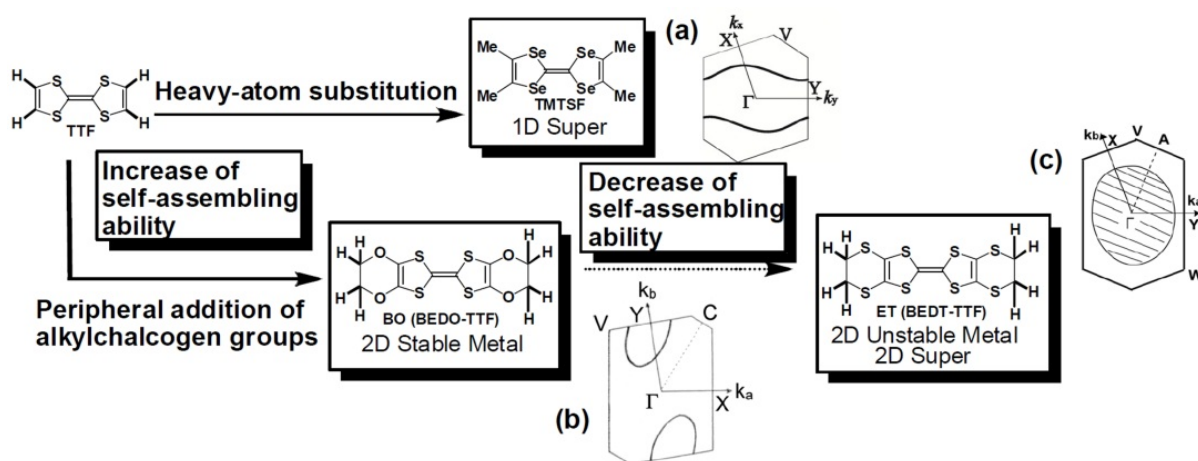

Figure 1. Strategy for chemical modification of the TTF molecule to increase (arrows) or decrease (dotted arrow) the electronic dimensionality by the aid of enhancement or suppression of the self-assembling ability of the molecules, respectively [16]. Typical Fermi surfaces of TMTSF (a: (TMTSF)$_2$NbF$_6$), BO (b: (BO)$_{2.4}$I$_3$), and ET (c: β-(ET)$_2$I$_3$) CT solids are depicted.

In this review, we mainly introduce the development and present status of organic superconductors of CT type based on electron donor molecules such as ET, electron acceptor molecules such as C_{60} (highest T_c = 38 K at 0.7 GPa), aromatic hydrocarbons (highest T_c = 33 K at ambient pressure (AP)), $M(dmit)_2$ (highest T_c = 8.4 K at 0.45 GPa //b) and graphite (highest T_c = 15.1 K at 7.5 GPa), carbon nanotube (T_c ~ 15 K in zeolite), and B doped diamond (T_c = 11 K at AP). Besides those, single component organic compounds show superconductivity ($T_c \leq$ 2.3 K at 58 GPa). The most reported T_c values of CT solids of C_{60}, aromatic hydrocarbons, those recently prepared, and those under pressure are the on-set values that are approximately 0.5–1 K higher than the mid-point T_c values. All donor based superconductors are stable in open air, however, only $M(dmit)_2$ superconductors are stable among the acceptor based superconductors.

Most of the superconducting phases of TMTSF, ET, and C_{60} materials and also of oxide superconductors reside spin-ordered phases such as SDW and antiferromagnetic (AF) phases. We briefly describe the recent development of superconductors having superconducting phase next to spin-disorder state (quantum spin liquid state).

2. Preparation of organic superconductors

CT solids are prepared mainly by the following three redox reactions: (1) electrocrystallization (galvanostatic and potentiostatic), (2) direct reaction of donors (D) and acceptors (A) in the gaseous, liquid, or solid phase, and (3) metathesis usually in solution (D•X + M•A → D•A + MX, M: cation, X: anion). In the latter two cases, single crystals are produced by the diffusion, concentration, slow cooling, or slow cosublimation methods.

Electrocrystallization (main procedures in detail and corresponding references are described in Section 11 of Ref. 17) is performed with a variety of glass cells, as shown in Fig. 2. Strictly speaking, the potentiostatic method is the proper way, in which a three-compartments cell is employed and one of the compartments contains the reference electrode, such as saturated calomel or Ag/AgCl electrode. However, this method is troublesome when a large number of crystal-growth runs are performed for a long period of time due to the following: 1) the contamination through the use of a reference electrode cell, and 2) the limited space for the experiment. The galvanostatic method is much more convenient than the potentiostatic one from these points of view. An H-cell (20 ml or 50 ml capacity) and an Erlenmeyer-type cell (100 ml) with a fine- porosity glass-frit equipped with two platinum wire electrodes (1–5 mm in diameter) have been used (Fig. 2).

There are many factors and tricks to grow single crystals of good quality. The important factors besides both the purity and the concentration of the component materials are the kinds of solvent and electrolyte, the surface of the electrode, the current (0.5–5 μA), and temperature. THF (tetrahydrofuran), CH_2Cl_2, TCE (1,1,2-trichloroethane), chlorobenzene, CH_3CN, and benzonitrile are commonly utilized solvents. The addition of 1–10 v/v% ethanol occasionally accelerates the crystal growth. As for the electrolyte, solubility in organic solvent is an important factor and usual electrolytes are tetrabutylammonium (TBA) or tetraphenylphosphonium salt of anion X. Sometimes, the electrolyte is a combination of

soluble and insoluble materials. For example, single crystals of κ-(ET)$_2$Cu(NCS)$_2$ were prepared using 1) CuSCN + KSCN + 18-crown-6-ether, 2) TBA•SCN + CuSCN, or 3) Cu(NCS)$_2$•K(18-crown-6-ether). Low solubility of the components of the electrolyte in the specific solvent usually retarded single crystal growth. Ionic liquids such as 1-ethyl-3-methylimidazolium (EMI, Scheme 2) salts of X were found to afford single crystals of high quality, recently. Regarding the surfaces of electrodes each research group has special treatments such as burning (but not melting) or polishing with very fine powder. The electrode surface can be treated by applying a current to switch the polarity in a 1 M H$_2$SO$_4$ solution. When the radical species are unstable in solution, CT solids can be grown by applying a high current at very low temperatures; *e.g.*, salts of fluoranthene (–30 °C, 2 mA, Ni electrode), naphthalene, and azulene.
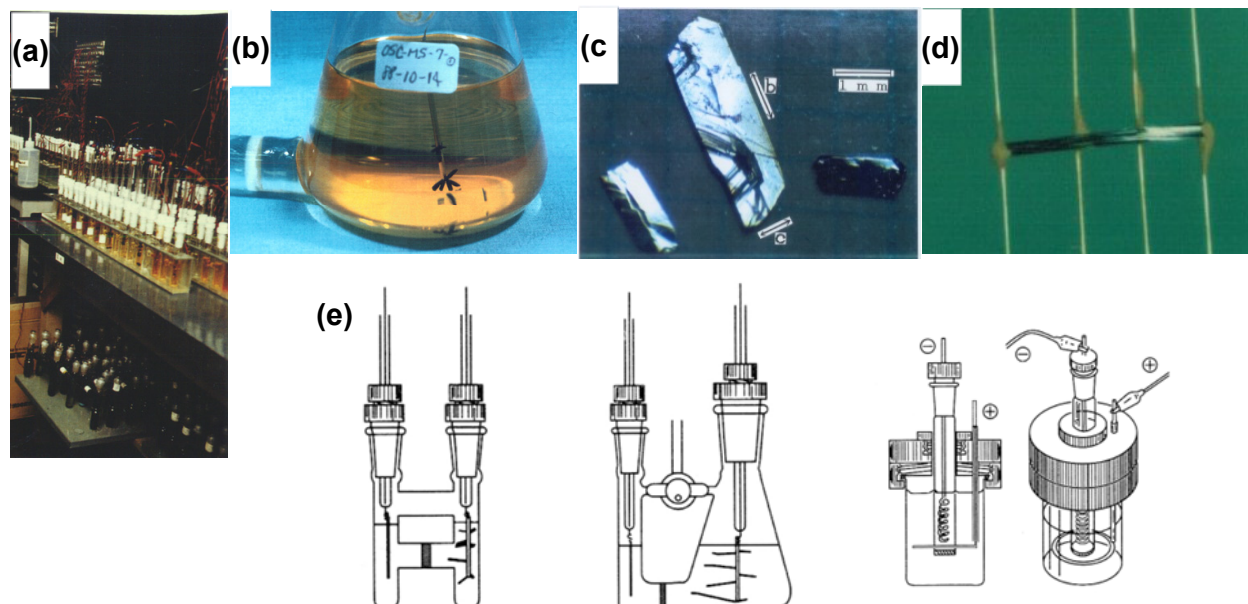

Figure 2. (a) Galvanostatic electrocrystallization using 20 ml cells on the desk. Under the desk the diffusion method is seen. (b) Single crystals of κ-(ET)$_2$Cu(NCS)$_2$ on the electrode in 100 ml cell and (c) showing two-dimensional conducting plane (*bc*). (d) Single crystal of (TMTSF)$_2$ClO$_4$ with four gold wires connected by gold paste. (e) Typical glass cells for electrocrystallization.

EMI
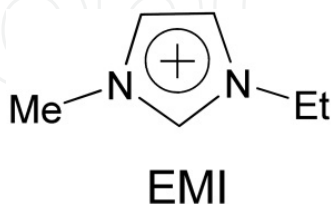
Scheme 2.

Besides the electrocrystallization, superconducting single crystals of good quality were prepared by direct chemical oxidation of ET with iodine in gas or with TBA•I$_3$ or TBA•IBr$_2$ in solution. Better-quality single crystals of (TTF)[Ni(dmit)$_2$]$_2$ were obtained by the diffusion method of the metathesis reaction rather than electrocrystallization. No single crystals of the electron acceptor based superconductors were obtained except for the M(dmit)$_2$ system.

The earliest route for reductive intercalation of C_{60} solids by alkali or alkaline-earth metals is the vapor-solid reaction by vacuum annealing. Almost all superconductors based on graphite and polyaromatic hydrocarbons have been obtained in accordance with this synthetic route. Besides pristine alkali metals, sodium mercury amalgams, sodium borohydride, alkali azides, and alkali decamethylmanganocene have been utilized for source of alkali metal vapors to reduce C_{60} solids. Disproportionation reaction between C_{60} and M_6C_{60} (M: alkali metal) has been sometimes utilized to obtain superconducting M_3C_{60} or non-superconducting M_4C_{60}. For a low-temperature solution route, liquid ammonia and methylamine have been sometimes utilized for the reaction media. Especially, Cs_3C_{60} with the highest T_c among the C_{60} superconductors can be obtained only when the stoichiometric amounts of cesium metal and C_{60} were reacted in the dissolved methylamine media (see Section 3-2), while the conventional vapor-solid reaction gives energetically stable Cs_1C_{60} and Cs_4C_{60} instead of Cs_3C_{60} with nominal composition.

3. Structures and properties

3.1. Superconductors based on electron donors

3.1.1. One-dimensional superconductors (TMTSF and TMTTF families)

TMTSF [9–14] has provided eight quasi-one-dimensional superconductors; $(TMTSF)_2X$ with highest $T_c \sim 3$ K [11] (Table 1). Most of them were prepared by electrocrystallization using TBA•X as electrolyte except the NbF_6 salt which can be only prepared by using ionic liquid EMI·NbF_6 [12]. They are isostructural to each other and the crystal structure of $(TMTSF)_2NbF_6$ is depicted in Fig. 3, where TMTSF molecules form a zigzag dimer that forms a segregated column along the face-to-face direction (a-axis) with no short Se···Se atomic contacts (Fig. 3a,3b). Along the side-by-side direction (b-axis), rather short Se···Se atomic contacts were seen (Fig. 3c), however, those less than the sum of the van der Waals radii (3.80 Å) are present only for X = ClO_4 and FSO_3. For the PF_6 salt, t_a and t_b were estimated to be 0.25–0.30 eV and 0.031 eV, respectively. Consequently, the Fermi surface of $(TMTSF)_2X$ is not closed, but open with fair warping due to the lack of adequate side-by-side transfer interactions (Fig. 1a).
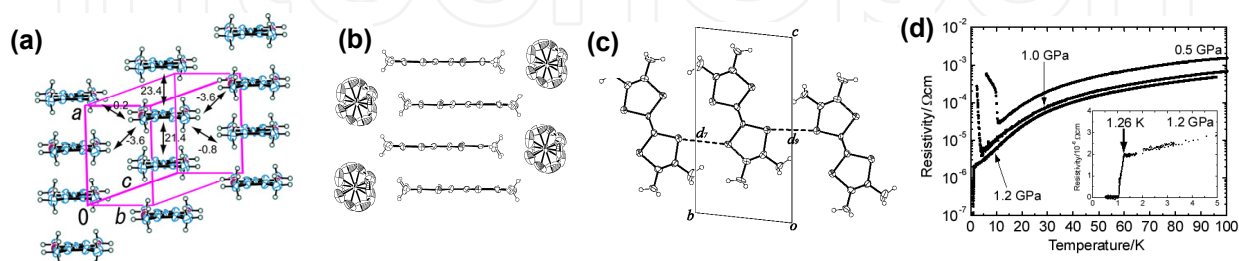

Figure 3. Crystal structure of $(TMTSF)_2NbF_6$ [12]. (a) Segregated column of TMTSF molecules. The numbers indicate the overlap integrals in 10^{-3} units. (b) Zigzag stacking of the TMTSF column. (c) Se···Se atomic contacts (d_7, d_9) along the side-by-side direction. (d) Temperature dependence of resistivity under pressure.

Salts with octahedral anions exhibited MI transition at 11–17 K at AP due to SDW, and a superconductivity appeared with on-set T_c of ca. 1 K at 0.6–1.2 GPa (Fig. 3d). Salts with (pseudo)tetrahedral anions, on the other hand, exhibited order-disorder (OD) transition of anion molecules when the superlattice created was coincide with the nesting vector of the warped Fermi surface ($2a \times 2b$, Fig. 1a).

The isomorphous (TMTTF)$_2$X (TMTTF: Scheme 3) salts displayed superconductivity under high pressure of 2.6–9 GPa with T_c less than 3 K for X = Br, BF$_4$, PF$_6$, and SbF$_6$ [22–25]. Table 1 summarizes superconductors of (TMTSF)$_2$X and (TMTTF)$_2$X showing σ_{RT}, temperature at which conductivity shows maximum (T_{max}) due to an MI transition, critical pressure to induce superconductivity (P_c), T_c, phenomena which cause the MI transition (transition temperature), and superlattice after the ordering of the anion molecules.

(TMTSF)$_2$ClO$_4$ is the only AP superconductor among them and shows no Hebel-Slichter coherence peak [26], which should be observed just below T_c for a normal BCS-type superconductor having an isotropic gap [27], in the early measurements of relaxation rate of ^{1}H NMR absorption. Later, the thermal conductivity suggested a fully-gapped order parameter [28]. The superconducting coherent lengths are 710 ($//a$), 340 ($//b$), and 20 Å ($//c$), indicating a quasi-one-dimensional character. The application of magnetic field breaks the superconducting state and induces a sequence of SDW (field-induced SDW: FISDW) states above 3 T. Upper critical magnetic field H_{c2} of the PF$_6$ salt (H_{c2} = 6 ($//b'$), 4 ($//a$) T at 0.1 K) is far beyond the Pauli limit (H_{Pauli}) for the BCS-type superconductor with weak coupling [10]. A generalized phase diagram including (TMTSF)$_2$X and (TMTTF)$_2$X indicates that the superconducting phase neighbors the magnetic SDW phase (Fig. 4) [29].
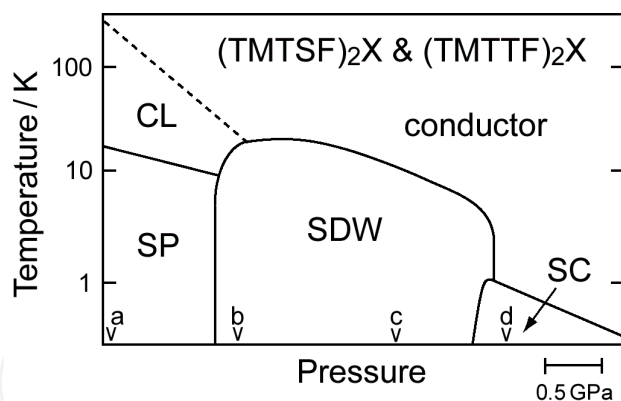
Figure 4. Generalized phase diagram for the (TMTSF)$_2$X and (TMTTF)$_2$X [29]. CL, SP, and SC refer to charge-localized (which corresponds to charge-ordered state), spin-Peierls, and superconducting states, respectively. The salts **a–d** at AP locates in the generalized diagram. **a**: (TMTTF)$_2$PF$_6$, **b**: (TMTTF)$_2$Br, **c**: (TMTSF)$_2$PF$_6$, **d**: (TMTSF)$_2$ClO$_4$.
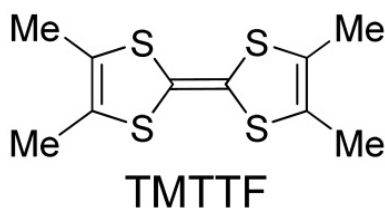
Scheme 3.

X	Symmetry	σ_{RT} / S cm^{-1}	T_{max}[a)] / K	P_c / GPa	T_c[b)] / K	Characteristics[c)]
TMTSF system						
PF$_6$	octahedral	540	12-15	0.65	1.1	SDW (12 K), FISDW
AsF$_6$	octahedral	430	12-15	0.95	1.1	SDW (12 K, J = 604 K)
SbF$_6$	octahedral	500	12-17	1.05	0.38	SDW (17 K)
NbF$_6$	octahedral	120	12	1.2	1.26	SDW (12 K)
TaF$_6$	octahedral	300	15	1.1	1.35	SDW (11 K)
ClO$_4$	tetrahedral	700	–	0	1.4	OD (24 K, $a \times 2b \times 2c$), FISDW, (γ = 10.5, β = 11.4, $\varTheta$ = 213)
		–	5	–	–	SDW (5 K) by rapid cool
ReO$_4$	tetrahedral	300	~182	0.95	1.2	OD (177 K, $a \times 2b \times 2c$)
FSO$_3$	pseudo-tetrahedral	1000	~88	0.5	3	OD (88 K, $a \times 2b \times 2c$)
TMTTF system						
PF$_6$	octahedral	20	245	5.2-5.4	1.4-1.8	spin-Peierls (15 K)
SbF$_6$	octahedral	8	150	5.4-9	2.8	charge-order, AF (8 K)
BF$_4$	tetrahedral	50	190	3.35-3.75	1.38	OD (40 K), SDW and SC (coexist)
Br	spherical	260	100	2.6	1.0	AF (15 K)

a) T_{max}: temperature at maximum conductivity. b) T_c: on-set. c) SDW: spin density wave, OD: order-disorder transition of anion and newly formed superlattice. FISDW: field-induced SDW. γ and β are important quantities experimentally determined to obtain $D(\varepsilon_F)$ (eq. 1) and $\varTheta$ (eq. 2) which are related with T_c by eq. 3 for the BCS-type superconductors.

Table 1. Organic superconductors of (TMTSF)$_2$X and (TMTTF)$_2$X

γ: Sommerfeld coefficient, mJ mol^{-1} K^{-2}

$$\gamma = \pi^2 k_B^2 D(\varepsilon_F)/3 \tag{1}$$

β: mJ mol^{-1} K^{-4}

$$\beta = 48\pi N k_B/5\varTheta^3 \tag{2}$$

$\varTheta$: Debye temperature, K

$$T_c \propto \varTheta \exp(-1/V_{el\text{-}ph}D(\varepsilon_F)) \tag{3}$$

k_B: Boltzmann constant, g: coupling constant, $V_{el\text{-}ph}$: electron-phonon coupling potential, $D(\varepsilon_F)$: density of states at Fermi level per one spin.

3.1.2. Two-dimensional superconductors (BO, ET, and BETS families)

3.1.2.1. BO superconductors

TTF derivatives with "peripheral addition of alkylchalcogeno groups" were found to be effective to increase dimensionality of CT solids and suppress the Peierls-type MI transition for many BO [15] and ET [16–20] conductors. The robust intermolecular interactions in the BO complexes have provided a metallic state even in the strongly disordered systems. The

strong two-dimensionality in the BO complexes hardly exhibited any phase transition including the superconductivity (only two superconductors with $T_c \leq 1.5$ K were found) [30,31].

3.1.2.2. ET superconductors

The first ET two-dimensional organic metal down to low temperatures is $(ET)_2(ClO_4)(TCE)$ [32]. Since then, hundreds of ET solids have been prepared. ET molecules tend to pile up one after the other with sliding to each other so as to minimize the steric hindrance caused by the terminal ethylene groups. A neutral ET molecule is non-planar and becomes almost flat on formation of the partial CT complex except the terminal ethylene groups which are thermally disordered at high temperatures. Segregated packing of such molecules leaves cavities along the molecular long axis, where counter anions and sometimes solvent molecules occupy. It was pointed out that the ethylene conformation is one of the key parameters determining the physical and structural properties including the superconductivity [33]. ET molecule also has a strong tendency to form proximate intermolecular S···S contacts along the side-by-side direction leading to an increment of the side-by-side transfer integrals $t_\perp$ (Fig. 5). The ET conductors are composed of alternating structures of two-dimensional conducting layer and insulating anion layer. Significant donor···anion interactions arise from the short atomic contacts between the ethylene hydrogen atoms of ET and anion atoms around the anion openings in the anion layer as schematically shown in Fig. 5b [34].
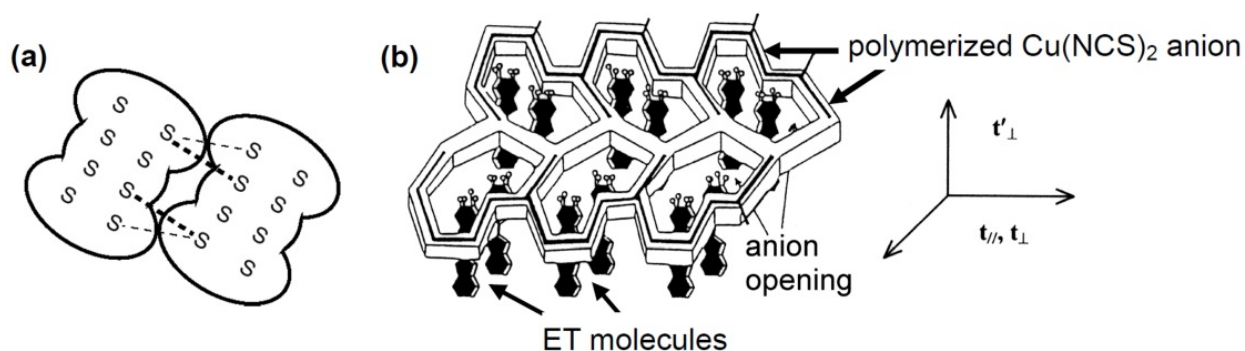

Figure 5. (a) Schematic figure of an example of S···S atomic contacts observed in ET salts. Thick dotted lines: S_{in}···S_{out}. Thin dotted lines: S_{out}···S_{out}. (b). Schematic view of κ-$(ET)_2Cu(NCS)_2$ indicating anion openings and transfer interactions ($t_{//}$, $t_\perp$, and $t'_\perp$) [34]. ET dimers are nearly orthogonally aligned (κ-type packing). For κ-type salt, $t_{//} \sim t_\perp \gg t'_\perp$.

The steric hindrance exerted by bulky six-membered rings of ET molecules prevents the formation of intermolecular S_{in}···S_{in} contacts (S_{in}: sulfur atom in the TTF skeleton, Fig. 5a). No particular patterns of intermolecular S_{in}···S_{out} (S_{out}: sulfur atom in the six-membered ring) are favorable as well. As a consequence various kinds of S···S contacts are produced depending on the donor packing patterns (α-, β-, θ-, κ-phases, and so forth, see Section 3-1-2-5), and are comparable to the other intermolecular interactions; i.e., face-to-face (π-π) and donor···anion interactions. Any interactions could not solely determine the donor packing picture. It is thus much more difficult to predict the donor packing pattern for the ET system compared

to those for TMTSF, especially for salts with small and discrete anions such as I_3, ClO_4, PF_6, etc., where polymorphic isomers are frequently afforded. In the salts with discrete linear anions such as I_3 and I_2Br, the component molecules have great freedom of motion and the donor packing pattern can be changed by thermal or pressure treatment [35,36]. Scanning tunneling microscope (STM) measurements [37–39] revealed that the surface structure of β-$(ET)_2I_3$ crystals contains many defects, voids, and reconstruction of donor packing attributed to the unstable structure of the anion layers, while the surface structures of salts with polymerized anions such as κ-$(ET)_2Cu(NCS)_2$ (Fig. 7b in Section 3-1-2-3) and α-$(ET)_2MHg(SCN)_4$ (M = NH_4 and K) are stable with no defects.

The polymerized anions in κ-$(ET)_2Cu(NCS)_2$ form the insulating layer having openings as seen in Fig. 5b. Two ET molecules form a dimer unit which fits into each opening. In more accurate description, the hydrogen atom of one ethylene group of ET molecule fits into the core created by anion molecules, like a key-keyhole relation. The position of such an ethylene hydrogen atom projected onto the anion cores produces unique patterns; called α-type (5 superconductors), β-type (6 superconductors), θ-type (1 superconductor), and κ-type (about 31 superconductors) [40]. It means that the ET molecules arrange according to the anion core or opening pattern created by polymerized anions.

Different kinds of ET···ET (π-π, S···S) and ET···anion (hydrogen bonds) intermolecular interactions, large conformational freedom of ethylene groups, flexible molecular framework, fairly narrow bandwidth (*W*), and strong electron correlations, which are represented by on-site Coulomb repulsion energy *U*, gave a rich variety of complexes with different crystal and electronic structures ranging from insulators to superconductors (corresponding references are cited in Ref. 16): Mott insulators (including spin-Peierls systems, antiferromagnets, spin-ladder systems, and quantum spin liquid), one-dimensional metals with CDW transition, two-dimensional metals with CDW transition, two-dimensional metals with FISDW transition, charge-ordered insulators, monotropic complex isomers, and two-dimensional metals down to low temperatures.

About 60 ET superconductors have so far been known. Table 2 summarizes selected ET superconductors and related salts. They are classified into three classes based on the transport behavior at AP: 1) Salts in Class I are metallic down to rather low T_c. 2) Salts in Class II are close to a Mott insulator and a poor metal showing $T_c > 10$ K. 3) Salts in Class III are insulators (Mott, CDW, or charge order). Figure 6 compares the temperature dependence of resistivity for several κ-$(ET)_2X$ with that of β-$(ET)_2AuI_2$ (**6**, Class I) which exhibited metallic behavior down to T_c at 4.9 K [48]. κ-$(ET)_2Cu(CN)[N(CN)_2]$ [49] (**1**, Class II) showed a monotonous decrease of resistivity with upper curvature down to T_c. κ-$(ET)_2Cu[N(CN)_2]Br$ [55] (**3**, Class II) exhibited similar behavior to that of κ-$(ET)_2Cu(NCS)_2$ [51] (**2**, Class II) except a metallic regime near RT in 2. They have a semiconductive region down to 70–80 K followed by a metallic behavior down to T_c. κ-$(ET)_2Cu[N(CN)_2]Cl$ [57–60] (**4**, Class III) ia a Mott insulator and showed a semiconductor (ε_g = 24 meV)-semiconductor (ε_g = 104 meV) transition at ca. 42 K due to an AF fluctuation resulting in a weak ferromagnet below 27 K (Néel temperature T_N = 27 K). Under a low pressure, it showed a similar temperature dependence to that of κ-$(ET)_2Cu[N(CN)_2]Br$. κ-$(ET)_2Cu_2(CN)_3$ [61–65] (**5**,

Class III) is semiconductive (a Mott insulator) and under pressure it also behaves similarly to **4** (semiconductor-metal-superconductor).
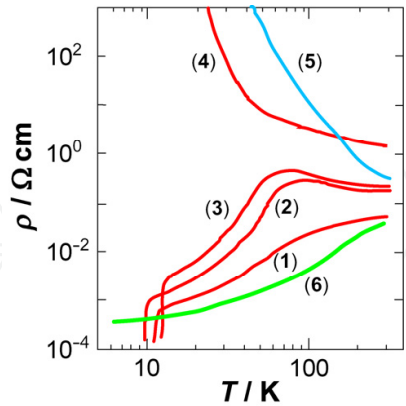

Figure 6. Temperature dependences of resistivity of 10 K class superconductors κ-(ET)$_2$Cu(CN)[N(CN)$_2$] (**1**), κ-(ET)$_2$Cu(NCS)$_2$ (**2**), κ-(ET)$_2$Cu[N(CN)$_2$]Br (**3**), and κ-(ET)$_2$Cu[N(CN)$_2$]Cl (**4**), which are compared with that of a good metal with low T_c β-(ET)$_2$AuI$_2$ (**6**) and a Mott insulator κ-(ET)$_2$Cu$_2$(CN)$_3$ (**5**) at AP.

Class, Salt		CuL$_1$L$_2$ L$_1$, L$_2$	σ_{RT}/ S cm^{-1}	$T_c^{a)}$ / K H-salt	D-salt	t'/t	U/W	Ground state at AP$^{b)}$	Characteristics, Quantum oscillations	Ref
I	κ-(ET)$_2$I$_3$		30	3.6*	–	0.58		SC	$\gamma = 18.9$, $\beta = 10.3$, $\Theta = 218$, SdH, dHvA	[41]
	β-(ET)$_2$I$_3$		60	1.5, 2.0, 8.1	–	0.55		SC	SdH, dHvA, AMRO	[42–47]
	6 β-(ET)$_2$AuI$_2$		20–60	4.9	–	–		SC	SdH, dHvA	[48]
II	**1** κ-(ET)$_2$Cu(CN)[N(CN)$_2$]	CN, N(CN)$_2$	5–50	11.2*	12.3*	0.66–0.71	0.87	SC	AMRO	[49,50]
	2 κ-(ET)$_2$Cu(NCS)$_2$	SCN, NCS	5–40	10.4*	11.2*	0.82–0.86	0.94	SC	$\gamma = 25$, $\beta = 11.2$, $\Theta = 215$, SdH, dHvA, AMRO	[51–54]
	3 κ-(ET)$_2$Cu[N(CN)$_2$]Br	N(CN)$_2$, Br	5–50	11.8*	11.2*	0.68	0.92	SC	$\gamma = 22$, $\beta = 12.8$, $\Theta = 210$, SdH, AMRO	[55,56]
III	**4** κ-(ET)$_2$Cu[N(CN)$_2$]Cl	N(CN)$_2$, Cl	2	12.8/0.03 GPa	13.1	0.75	0.90	AF	SdH, AMRO, $T_N = 27$ K	[57–60]
	5 κ-(ET)$_2$Cu$_2$(CN)$_3$	CN, CN/NC	2–7	6.8–7.3**	–		1.06	0.9	SL	SdH, AMRO	[49,61–65]
	ET•TCNQ		10			–		AF	$T_N = 3$ K	[66]
	β'-(ET)$_2$ICl$_2$		3×10^{-2}	14.2/8.2 GPa		–		AF	$T_N = 22$ K	[67,68]
	β'-(ET)$_2$AuCl$_2$		~10^{-1}			–		AF	$T_N = 28$ K	[68]
	β'-(ET)$_2$BrICl		~10^{-2}	7.2/8.0 GPa				AF	$T_N = 19.5$ K	[69]

a) *: mid-point. **on-set under uniaxial strain (see Fig. 9a). Others are the on-set values under hydrostatic pressure. b) SC: superconductor, SL: spin liquid.

Table 2. Selected ET conductors and superconductors. Except ET•TCNQ, the compound is represented by *Greek alphabet*-(ET)$_2$X (Greek alphabet: type of donor stacking, L$_1$, L$_2$: ligand). a) Class **I** : good metal with low T_c, **II**: 10 K class AP superconductor, **III**: Mott insulator. **1–6** are the numbers in Fig. 6.
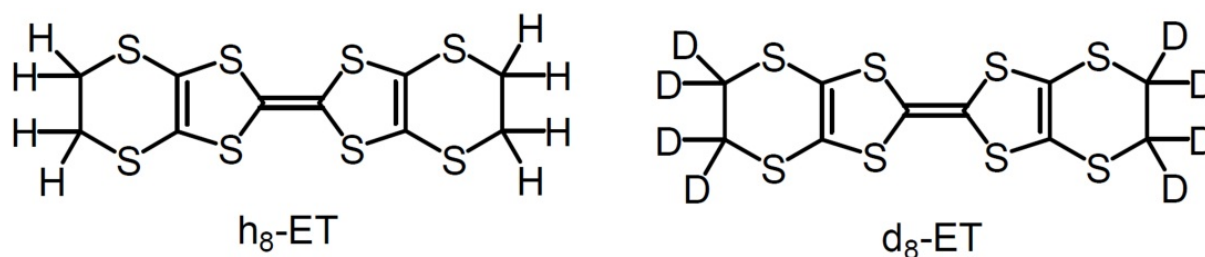
Scheme 4.

Table 2 summarizes T_c of H- and D-salts (salt using h8-ET and d8-ET, respectively; Scheme 4). The calculated U/W values close to unity suggest that those salts have strong electron correlation. Currently β'-(h8-ET)$_2$ICl$_2$ (on-set T_c = 14.2 K at 8.2 GPa [68], mid-point T_c of 13.4 K is estimated) and D-salt of **4** (T_c = 13.1 K at 0.03 GPa) [58] show the highest T_c under pressure, while both are Mott insulators at AP. At AP, D-salt of **1** shows the highest T_c of 12.3 K [50] followed by H-salt of **3** (T_c = 11.8 K) [55,56]. These salts are electronically clean metals as evidenced by the observation of quantum oscillations (Shubnikov-de Haas (SdH), de Haas-van Alphen (dHvA)), and geometrical oscillations: angular dependent magnetoresistance oscillation (AMRO), which afford topological information for the Fermi surface [19,20,70].

Next, we will focus mainly on the κ-type superconductors with polymerized anions.

3.1.2.3. κ-type ET conductors

The κ-type superconductors κ-(ET)$_2$CuL$_1$L$_2$ (**1–5** in Table 2) share some common structural and physical properties [49–65]. Figure 7 shows the crystal structure of the prototype H-salt of **2**, anion structures, donor packing pattern, and calculated Fermi surface [51–54]. Table 2 summarizes the two kinds of ligand (L$_1$, L$_2$) in a salt and ratio t'/t for triangle geometry of ET dimers. These salts have polymerized anions in which ligand L$_1$ forms infinite chain by coordinating to Cu^{1+} and ligand L$_2$ coordinates to Cu^{1+} as pendant. ET molecules form a dimer and the ET dimers are arranged nearly orthogonally to each other forming two-dimensional conducting ET layer in the bc-plane which is sandwiched by the insulating anion layers along the a-axis (Fig. 7a). Cu^{1+} and SCN form Cu···SCN···Cu···SCN··· zigzag infinite chain along the b-axis and other ligand SCN coordinates to Cu^{1+} by N atom to make an open space (indicated by ellipsoid in Fig. 7b, also see Fig. 5) to which an ET dimer fits. An ET dimer has one spin, and the dimers form triangle (Fig. 7c) whose shape is represented by the ratio t'/t (Fig. 7d).

H-salt of **4** showed a complicated T-P phase diagram (Fig. 8a) [72–76]. Thoroughgoing studies under pressure showed a firm evidence of the coexistence of superconducting (**I-SC-2** phase: **I-SC** = incomplete superconducting) and AF phases [72–78], where the radical electrons of ET molecules played both roles of localized and itinerant ones. Under a pressure of ca. 20–30 MPa another incomplete superconducting phase (**I-SC-1**) appeared and the complete superconducting (**C-SC**) phase neighbored to this phase at higher pressures. Below these superconducting phases, reentrant nonmetallic (**RN**) phase was observed. Similar T-P phase diagrams were obtained for κ-(d8-ET)$_2$X (X = Cu[N(CN)$_2$]Cl and

Cu[N(CN)$_2$]Br) with a parallel shift of pressure. They occur at the higher and lower pressure sides of the κ-(h$_8$-ET)$_2$Cu[N(CN)$_2$]Cl for the Br and Cl salts, respectively. Contrary to the H-salt, κ-(d$_8$-ET)$_2$Cu[N(CN)$_2$]Cl exhibited no coexistence of the superconducting and AF phases. At AP, κ-(ET)$_2$Cu[N(CN)$_2$]I is a semiconductive and becomes superconducting under hydrostatic pressure above 0.12 GPa with T_c of 7.7 K (on-set T_c = 8.2 K), though the magnetic ordering was not clarified at AP [79].
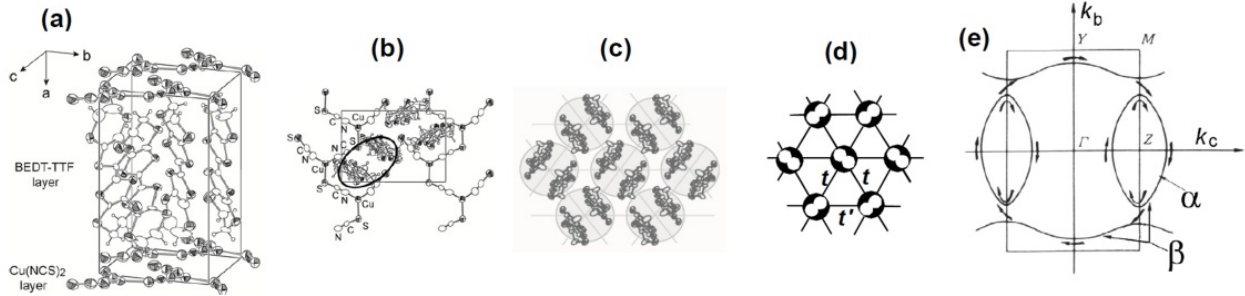

Figure 7. κ-(ET)$_2$Cu(NCS)$_2$: (a) Crystal structure. (b) Anion layer viewed along the a-axis has anion openings (indicated by ellipsoid) to which an ET dimer fits. Picture is the dextrorotatory form. (c) Packing pattern (κ-type) of ET dimers along the a-axis. (d) Schematic view of triangular lattice of ET dimers which has one spin. White and black circles represent ET molecule and ET dimer, respectively. The t'/t represents the shape of the triangle. (e) Calculated Fermi surfaces of the $P2_1$ salts (κ-(ET)$_2$Cu(NCS)$_2$, κ-(ET)$_2$Cu(CN)[N(CN)$_2$]) showed the certain energy gap between a one-dimensional electron like Fermi surface (//k_c) and a two-dimensional cylindrical hole-like one (α-orbit), while such a gap is absent in the $Pnma$ salts (κ-(ET)$_2$Cu[N(CN)$_2$]Br, κ-(ET)$_2$Cu[N(CN)$_2$]Cl). For κ-(ET)$_2$Cu(NCS)$_2$, electrons move along the closed ellipsoid (α-orbit) to exhibit SdH oscillations [53], and at higher magnetic field (> 20 T) electrons hop from the ellipsoid to open Fermi surface to show circular trajectory (β-orbit, magnetic breakdown oscillations) [71].
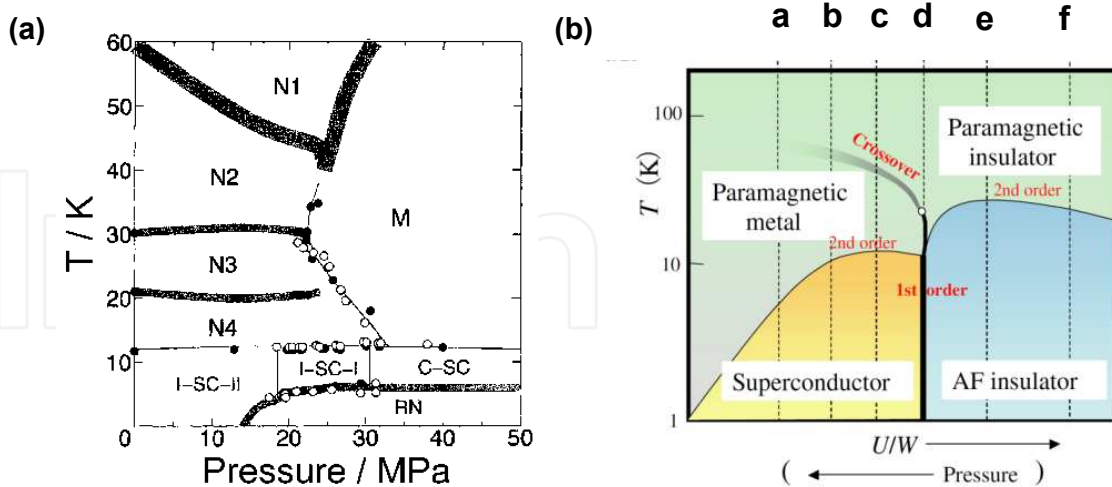

Figure 8. (a) Phase diagram of κ-(h$_8$-ET)$_2$Cu[N(CN)$_2$]Cl determined from electrical conductivity and magnetic measurements [72–76]. **N1–N4**: non-metallic phases, **M**: metallic phase, **RN**: reentrant non-metallic phase, **I-SC-I** and **I-SC-II**: incomplete superconducting phases. **N3** shows growth of three-dimensional AF ordered phase. **N4** is a weak ferromagnetic phase. (b) Proposed simplified phase diagram [80]. **a**: β-(ET)$_2$I$_3$, **b**: κ-(ET)$_2$Cu(NCS)$_2$, **c**: H-salt of κ-(ET)$_2$Cu[N(CN)$_2$]Br, **d**: D-salt of κ-(ET)$_2$[N(CN)$_2$]Br, **e**: κ-(ET)$_2$[N(CN)$_2$]Cl, **f**: β-(ET)$_2$ICl$_2$.

Alternating mixed donor packing motifs were observed in two phases of α'-κ-$(ET)_2Ag(CF_3)_4(TCE)$, T_c (on-set) of which are 9.5 K and 11.0 K for the phase having two-layered ($\alpha' + \kappa$) and four-layered ($\alpha' + \kappa_1 + \alpha' + \kappa_2$) phase, respectively [81,82]. Since α'-packing generally imparts semiconducting state, both systems have nano-scale hetero junction of semiconductive/superconductive interface, which is thought to give higher T_c in these systems in comparison with κ-$(ET)_2Cu(CF_3)_4(TCE)$ (T_c = 4.0 K). If this explanation is correct, this is an example of interface superconductivity [83,84].

With increasing the distance between the ET dimers in Fig. 7a–d, the transfer interactions between ET dimers decrease; this may correspond to the decrease of W and to increase of $D(\varepsilon_F)$, and consequently T_c is expected to increase. According to this line of thought, higher T_c is expected for the salt having a larger anion spacing. Such a κ-type salt may be found near the border between poor metals and Mott insulators. It is true not only for κ-type but also for other types, $e.g.$, β'-$(ET)_2X$ (X = ICl_2 [67,68] and BrICl [69]) having high T_c in the ET family are Mott insulators at AP.

Topological structures of their Fermi surfaces studied by SdH, dHvA, and AMRO (Table 2) [19,20,53,70,71,85–87] show that the area of the closed Fermi surface relative to the first Brillouin zone and cyclotron mass calculated from SdH oscillations are 15.7% (α-orbit in Fig. 7e, $3.5m_e$) and 105% (β-orbit in Fig. 7e, $6.5m_e$) for **2** at AP, 4.4% ($0.95m_e$) at 0.9 GPa and $ca.$ 100% ($6.7m_e$) at AP for **3**, and 15.5% ($1.7m_e$) and 102% ($3.5m_e$) at 0.6 GPa for **4**. Fermi surface of **2** (Fig. 7e) calculated based on the crystal structure is in good agreement with these observed data.

The followings are the superconducting characteristics of κ-type ET superconductors, some of which differ from those of the conventional BCS superconductors.

1. Upper critical magnetic field H_{c2}: **2** gave higher H_{c2} values for the magnetic field parallel to the two-dimensional plane than H_{Pauli} based on a simple BCS model [88,89].
2. Coherent length ξ: The superconducting coherent lengths are 29 and 3.1 Å for **2** at 0.5 K along the two-dimensional plane ($\xi_{//}$) and perpendicular to the plane ($\xi_\perp$). The $\xi_{//}$ is larger than the lattice constants, however, the $\xi_\perp$ is much smaller than the lattice constant indicating the conducting layers along this direction is Josephson coupled.
3. Symmetry of superconducting state: No Hebel-Slichter coherence peak was observed in both **2** and **3** in ^1H NMR measurements, ruling out the BCS s-wave state. The symmetry of the superconducting state of **2** had been controversially described as normal BCS-type or non-BCS type, however, STM spectroscopy showed the d-wave symmetry with line nodes along the direction near $\pi/4$ from the k_a- and k_c-axes ($d_{x^2-y^2}$) [90], and thermal conductivity measurements were consistent with that [91]. STM on **3** also showed the same symmetry [92]. A recent specific heat measuremen on **2** and **3** was consistent with these results [93].
4. Inverse isotope effect: Inverse isotope effect has so far been observed for **1** [50], **2** [54], and **4** [58], while normal isotope effect for **3** [56]. The reason of the observed isotope effects is not fully understood yet consistently.

5. A very simplified *T-P* phase diagram for κ-(ET)$_2$X was proposed (Fig. 8b), where only the parameter *U/W* is taken into account. Fig. 8b includes the salts **2**, **3**, **4**, β-(ET)$_2$I$_3$, and β'-(ET)$_2$ICl$_2$ [80], however, the metallic behavior of **2** above 270 K and that of **1**, whole behavior of **5**, and low-temperature reentrant behavior of **3** and **4** (Fig. 8a) cannot be allocated in this diagram. The β-(ET)$_2$I$_3$ in Fig. 8b should be β_H-phase ($T_c \sim$ 8 K, see Section 3-1-2-5) and other two β-(ET)$_2$I$_3$ salts of $T_c \sim$ 1.5 K and $\sim$2 K phases cannot be allocated though they should have the same *U/W* values. T_c of **4** is higher than that of β'-(ET)$_2$ICl$_2$ in Fig. 8b contrary to the experimentally observed T_c results. This phase diagram and "geometrical isotope effect" [94] point out that T_c's of β-(ET)$_2$I$_3$, **2**, and **3** decrease with increasing pressure if only the parameter *U/W* or $D(\varepsilon_F)$ is taken into account. This tendency has been observed under hydrostatic pressure but not under uniaxial pressure (see Sections 3-1-2-4, 3-1-2-5, 3-1-3). Thus the phase diagram in Fig. 8b remains incomplete, despite it is frequently used to explain the general trends for these salts.

3.1.2.4. Quantum spin liquid state in κ-(ET)$_2$Cu$_2$(CN)$_3$ and neighboring superconductivity

As mentioned, κ-type packing is characterized by the triangular spin-lattice (Fig. 7c,7d) where an ET dimer is a unit with S = 1/2 spin [95,96]. The line shape of ^{1}H NMR absorption of κ-(ET)$_2$Cu[N(CN)$_2$]Cl [60] exhibited a drastic change below 27 K owing to the formation of three-dimensional AF ordering. On the other hand, the absorption band of κ-(ET)$_2$Cu$_2$(CN)$_3$ remains almost invariant down to 32 mK indicating non-spin-ordered state: quantum spin liquid state [63]. The appearance of spin liquid state in κ-(ET)$_2$Cu$_2$(CN)$_3$ is the consequence of significant spin frustration in this salt (t'/t = 1.06) in comparison with the less frustrated AF state in κ-(ET)$_2$Cu[N(CN)$_2$]Cl (t'/t = 0.75).

It has long been predicted that the geometrical spin frustration of antiferromagnets caused by the spin correlation in particular spin geometry (triangle, tetrahedral, Kagome (Scheme 5), etc.) prevents the permanent ordering of spins. So the spins of Ising system with AF interaction in the equilateral triangle spin lattice will not show any long-range order even at 0 K, and hence the phase, namely quantum spin liquid phase, has high degeneracy [97]. Such spin liquid state has only been predicted theoretically [98], and a variety of ideal materials have been designed and examined for long [99–102]. Since the discovery of the spin liquid state in κ-(ET)$_2$Cu$_2$(CN)$_3$, several materials have been reported to have such exotic spin state: EtMe$_3$Sb[Pd(dmit)$_2$]$_2$ [103], ZnCu$_3$(OH)$_6$Cl$_2$ [104,105], Na$_4$Ir$_3$O$_8$ [106], and BaCu$_3$V$_2$O$_8$(OH)$_2$ [107,108]. Some inorganic materials reported as spin liquid candidates were eliminated owing to the spin ordering at extremely low temperatures, etc [109–113]. Na$_4$Ir$_3$O$_8$ and two organic compounds (κ-(ET)$_2$Cu$_2$(CN)$_3$, EtMe$_3$Sb[Pd(dmit)$_2$]$_2$) may be recognized as "soft" Mott insulators and have metallic state under pressure. Only κ-(ET)$_2$Cu$_2$(CN)$_3$ has the superconducting phase next to spin-liquid state so far as described below.

The phase diagrams of TMTSF (Fig. 4), ET (Fig. 8), C$_{60}$ [114] families and also electron-correlated cuprate and iron pnictide high T_c systems [115] indicate that a magnetic ordered state (SDW, AF) is allocated next to the superconducting state. Figure 9a shows the *T-P* phase diagram of κ-(ET)$_2$Cu$_2$(CN)$_3$ at low temperature region by applying uniaxial strain along *c*- (t'/t decreases in this direction) and *b*- (t'/t increases in this direction) axes with

epoxy-method [62,65]. In both cases, a superconducting state readily appeared nearly above 0.1 GPa since the t'/t deviates from unity; *i.e.*, strong spin frustration was released. It is very noteworthy that the spin liquid phase is neighboring to the superconducting state and its T_c is fairly anisotropic as shown in Fig. 9b. A plot of T_c vs. T_{IM}, which is a Mott insulator-metal transition temperature, indicates that in comparison with the hydrostatic pressure results, the uniaxial method afforded: 1) a much higher T_c value, 2) an increase of T_c at the initial pressure region, 3) an anisotropic pressure dependence, and 4) superconducting phase remains at higher pressure. The uniaxial strain experiments including other κ-type superconductors clearly revealed that the T_c increased as the U/W approaches unity and as the t'/t departs from unity [116].
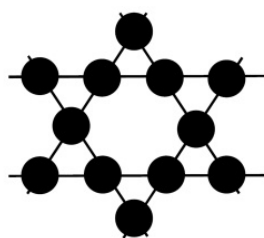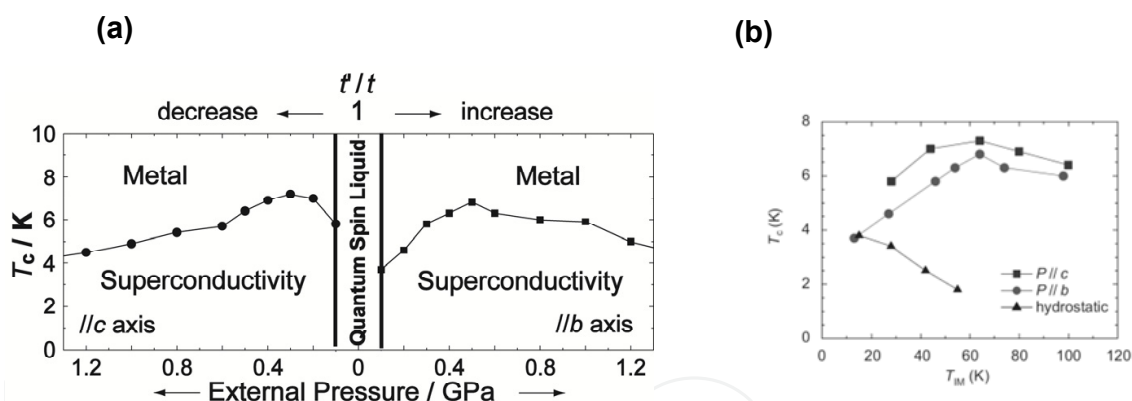

Kagome lattice

Scheme 5.

(a)   **(b)**

Figure 9. a) Temperature-uniaxial pressure phase diagram in the low temperature region of κ-(ET)$_2$Cu$_2$(CN)$_3$ [62,65]. The strain along the c-axis corresponds to a decrease of t'/t (left side), while the strain along the b-axis increases t'/t (right side). b) Pressure dependence of on-set T_c by the uniaxial strain and hydrostatic pressure methods. T_{IM}: a Mott insulator-metal transition temperature [65].

3.1.2.5. Other ET superconductors

One of the most intriguing ET superconductors is the salt with I$_3$ anion, which afforded α-, α_t-, β_L-, β_H-, δ-, ε-, γ-, θ-, and κ-type salts with different crystal and electronic structures. Among them, α-, α_t-, β_L-, β_H-, γ-, θ-, and κ-type salts are superconductors with T_c = 7.2, ~8, 1.5, 8.1, 2.5, 3.6, and 3.6 K, respectively [36,41,42,44,45,117–120]. The β_L-salt was converted to the β_H-salt by pressurizing (hydrostatic pressure) above 0.04 GPa and then by depressurizing while keeping the sample below 125 K [45,46]. The β_H-salt returned to β_L-salt when the salt was kept above 125 K at AP. The β_L-salt is characterized by having a

superlattice appearing at 175 K with incommensurate modulations of ET and I_3 to each other [121]. The formation of the superlattice was suppressed by the pressure above 0.04 GPa. Then the two ethylene groups in an ET molecule were fixed in the eclipsed conformation to give rise to more than 5 times higher T_c in β_H-salt. The T_c of β_H-salt decreased with increasing hydrostatic pressure monotonously, however, under the uniaxial stress the further T_c increase taking a maximum at a piston pressure of 0.3–0.4 GPa is observed for both directions parallel and perpendicular to the donor stack [120]. The superconducting coherent lengths are $\xi_{//}$ = 630 (//a) – 610 Å (//b') and $\xi_\perp$ = 29 Å (//c^*) for the β_L-salt, and $\xi_{//}$ = 130 Å and $\xi_\perp$ = 10 Å for the β_H-salt.

The α-(ET)$_2$I$_3$ exhibited nearly temperature independent resistivity down to 135 K, at which charge-ordered MI transition occurred [122,123]. It has been claimed that α-(ET)$_2$I$_3$ has a zero-gap state with a Dirac cone type energy dispersion like graphene [124,125]. Under hydrostatic pressure it became two-dimensional metal down to low temperatures (2 GPa), however, it became superconductor under the uniaxial pressure along the a-axis (0.2 GPa, on-set T_c = 7.2 K), though along the b-axis it remained metal down to low temperature (0.3–0.5 GPa) [117]. α-(ET)$_2$I$_3$ was able to be converted to mosaic polycrystal with $T_c \sim$ 8 K by tempering at 70–100 °C for more than 3 days, giving α_t-salt which exhibited similar NMR pattern to that of the β_H-salt [36]. Other α-type superconductors (α-(ET)$_2$MHg(SCN)$_4$: M = K, NH$_4$, Rb, Tl) seem to have charge-ordered state near or next to the superconducting state with low T_c (highest T_c = 1.7 K for M = NH$_4$). Uniaxial strain increased T_c anisotropically (6 K at 0.5 GPa //c, 4.5 K at 1 GPa //b^* for M = NH$_4$) [126]. The salts α-(ET)$_2$MHg(SCN)$_4$ were confirmed to retain their donor packing patterns under pressure at low temperature by the SdH observation. However, for α-(ET)$_2$I$_3$ under pressure at low temperature, no exact information is reported for the donor packing in the superconducting state.

Only one θ-type superconductor, θ-(ET)$_2$I$_3$, is known, however, one third of the obtained crystals are superconducting and others remain metallic [127]. Several θ-type salts are arranged by their inter-column transfer interactions, and the dihedral angle between columns in a phase diagram showing superconducting θ-(ET)$_2$I$_3$ is next to both the charge ordered state of θ-(ET)$_2$MM′(SCN)$_4$ (M = Tl, Rb, Cs, M′ = Zn, Co) and metallic phase of θ-(ET)$_2$Ag(CN)$_2$ [128]. It is not clear which point the non-superconducting θ-(ET)$_2$I$_3$ occupies in this phase diagram. Tempering (70 °C, 2 h) all crystals of θ-(ET)$_2$I$_3$ induced superconductivity with higher T_c (named θ_T-(ET)$_2$I$_3$: sharp drop of resistivity at 7 K and dull drop at ~5 K) [129]. The tempering changed the ethylene conformation and position of I_3 from disordered state in θ-phase to ordered state in θ_T–phase. Therefore, the phase diagram of the θ-type salts needs further parameters concerning with the structure of the salts (ethylene conformation and position or disorder of anions).

3.1.2.6. BETS superconductors

The most intriguing phenomenon among the 8 BETS (Scheme 6) superconductors (highest T_c = 5.5 K) is the reentrant superconductor-insulator-superconductor transition under magnetic field for (BETS)$_2$FeCl$_4$. The λ- or κ-type BETS salts formed with tetrahedral anions FeX$_4$ (X: Cl and Br) were studied in terms of the competition of magnetic ordering and

superconductivity [130–136]. The λ-(BETS)$_2$FeCl$_4$ exhibited coupled AF and MI transitions at 8.3 K. For the FeCl$_4$ salt, a relaxor ferroelectric behavior in the metallic state below 70 K [133] and a firm nonlinear electrical transport associated with the negative resistance effect in the magnetic ordered state have been observed [135]. Moreover it has been found that the FeCl$_4$ salt shows the field-induced superconducting transition under a magnetic field of 18–41 T applied exactly parallel to the conducting layers [132]. The λ-(BETS)$_2$Fe$_x$Ga$_{1-x}$X$_4$ passes through a superconducting to insulating transition on cooling [135]. The κ-(BETS)$_2$FeX$_4$ (X = Cl, Br) are AF superconductors (T_N = 2.5 K, T_c = 1.1 K for X = Br: T_N = 0.45 K, T_c = 0.17 K for X = Cl) [136]. Similar phenomena, namely AF, ferromagnetic, or field-induced superconductivity, have been observed in several inorganic solids such as Chevrel phase [137] and heavy-fermion system [138]. Recently it has been reported that λ-(BETS)$_2$GaCl$_4$ (T_c = 8 K(on-set), 5.5 K(mid-point)) exhibited superconductivity in the minute size of four pairs of (BETS)$_2$GaCl$_4$ based on the STM study [139]. This salt has two-dimensional superconducting character ($\xi_{/\!/}$ = 125 Å, $\xi_\perp$ = 16 Å).
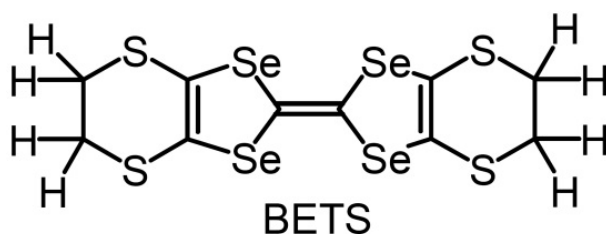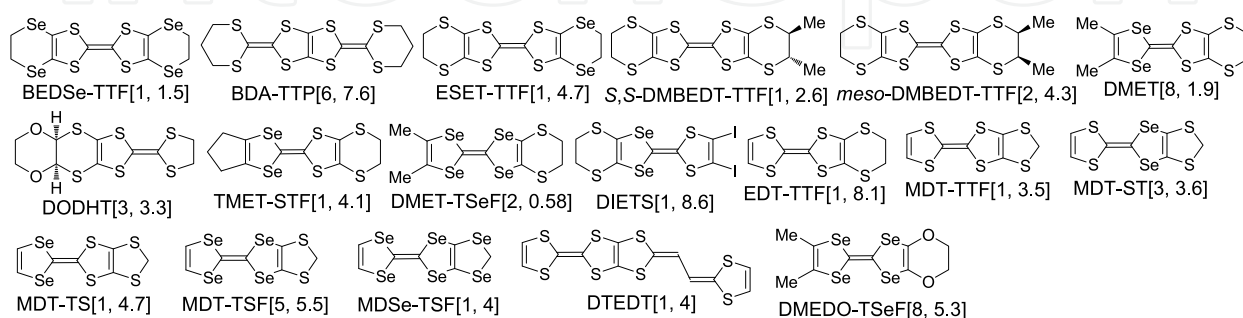

BETS

Scheme 6.

3.1.3. Superconductors of other electron donor molecules

Besides TMTSF, TMTTF, BO, ET, and BETS superconductors, there are other superconductors (Scheme 7, numbers in bracket are the total members of each superconducting family and the highest T_c) of CT salts based on symmetric (BEDSe-TTF [140] and BDA-TTP [141–144]) and asymmetric donors (ESET-TTF [145], S,S-DMBEDT-TTF [146], *meso*-DMBEDT-TTF [147,148], DMET [149], DODHT [150], TMET-STF [151], DMET-TSF [152], DIETS [153], EDT-TTF [154], MDT-TTF [155,156], MDT-ST [157,158], MDT-TS [159], MDT-TSF [160–163], MDSe-TSF [164], DTEDT [165], and DMEDO-TSeF [166,167]).

Donor Molecule

Scheme 7. Donor molecules for organic superconductors except TMTSF, TMTTF, BO, ET, and BETS systems. Numbers in bracket are the total members of each superconductor and the highest T_c.

κ-(MDT-TTF)$_2$AuI$_2$ (T_c = 3.5 K) exhibited a Hebel-Slichter coherent peak just below T_c, indicating a BCS-type gap with s-symmetry [156]. On the other hand, d-wave like superconductivity has been suggested for β-(BDA-TTP)$_2$SbF$_6$ [143,144]. β-(BDA-TTP)$_2$X (X = SbF$_6$, AsF$_6$) exhibited a slight T_c increase at the initial stage of uniaxial strain parallel to the donor stack and interlayer direction while T_c decreased perpendicular to the donor stack [142]. θ-(DIETS)$_2$[Au(CN)$_4$] exhibited superconductivity under uniaxial strain parallel to the c-axis (T_c = 8.6 K at 1 GPa), though under hydrostatic pressure a sharp MI transition remained even at 1.8 GPa [153]. MDT-ST, MDT-TS, and MDT-TSF superconductors [157–163] have non-integer ratio of donor and anion molecules such as (MDT-TS)(AuI$_2$)$_{0.441}$ making the Fermi level different from the conventional 3/4 filled band for TMTSF and ET 2:1 salts. The Fermi surface topology of (MDT-TSF)X (X = (AuI$_2$)$_{0.436}$, (I$_3$)$_{0.422}$) and (MDT-ST)(I$_3$)$_{0.417}$ has been studied by SdH and AMRO [158,161–163]. DMEDO-TSeF afforded eight superconductors. Six of them are κ-(DMEDO-TSeF)$_2$[Au(CN)$_2$](solvent) and the T_c's of them (1.7–5.3 K) are tuned by the use of cyclic ethers as solvent of crystallization [167]. The superconducting coherent lengths indicate that β-(BDA-TTP)$_2$SbF$_6$ has two-dimensional character ($\xi_{//}$ = 105 Å, $\xi_{\perp}$ = 26 Å) while (DMET-TSeF)$_2$AuI$_2$ has quasi-one-dimensional character (1000, 400, and 20 Å).

3.2. Superconductors based on electron acceptors

Icosahedral C$_{60}$ molecule with I_h symmetry has triply degenerate LUMO and LUMO+1 orbitals with t_{1u} and t_{1g} symmetries, respectively. In 1991, superconducting phase was observed below 19 K for the potassium-doped compounds prepared by a vapor-solid reaction [168], immediately after the isolation of macroscopic quantities of C$_{60}$ solid [169]. Powder X-ray diffraction profile revealed that the composition of the superconducting phase is K$_3$C$_{60}$ and the diffraction pattern can be indexed to be a face-centered cubic (fcc) structure [170]. The lattice constant (a = 14.24 Å) is apparently expanded relative to the undoped cubic C$_{60}$ (a = 14.17 Å). The superconductivity has been observed for many M$_3$C$_{60}$ (M: alkali metal), $e.g.$, Rb$_3$C$_{60}$ (T_c = 29 K [171]), Rb$_2$CsC$_{60}$ (T_c = 31 K [172]), and RbCs$_2$C$_{60}$ (T_c = 33 K [172]), and their structures determined to be analogous to that of K$_3$C$_{60}$ with varying lattice constants. The T_c varies monotonously with lattice constant, independently of the type of the alkali dopant (Fig. 10) [172,173]. The observation of a Hebel-Slichter peak in relaxation rate just below T_c in NMR [174] and μSR [175] indicate the BCS-type isotopic gap. The decrease in T_c due to the isotopic substitution [176] also supports the phonon-mediated pairing in M$_3$C$_{60}$, where the α value in $T_c \propto$ (mass)$^{-\alpha}$ (ideal value of α predicted by the BCS model is 0.5) is estimated to be 0.30(6) for K$_3^{13}$C$_{60}$ and 0.30(5) for Rb$_3^{13}$C$_{60}$.

Keeping the C$_{60}$ valence invariant (–3), the intercalation of NH$_3$ molecules ($e.g.$, (NH$_3$)K$_3$C$_{60}$) results in the lattice distortion from cubic to orthorhombic accompanied by the appearance of AF ordering instead of superconductivity [177]. Changing the valence in cubic system also has a pronounced effect on T_c. For example, T_c in Rb$_{3-x}$Cs$_x$C$_{60}$ prepared in liquid ammonia gradually increases as the mixing ratio approaches to x = 2 [178]. Further increasing the nominal ratio of Cs leads to a sizable decrease of T_c, despite the lattice keeps

the fcc structure for $x < 2.65$. Such a band-filling control has been realized for $Na_2Cs_xC_{60}$ ($0 \leq x \leq 1$) [179] and Li_xCsC_{60} ($2 \leq x \leq 6$) [180], and shows that the T_c decreases sharply as the valence state on C_{60} deviates from -3.
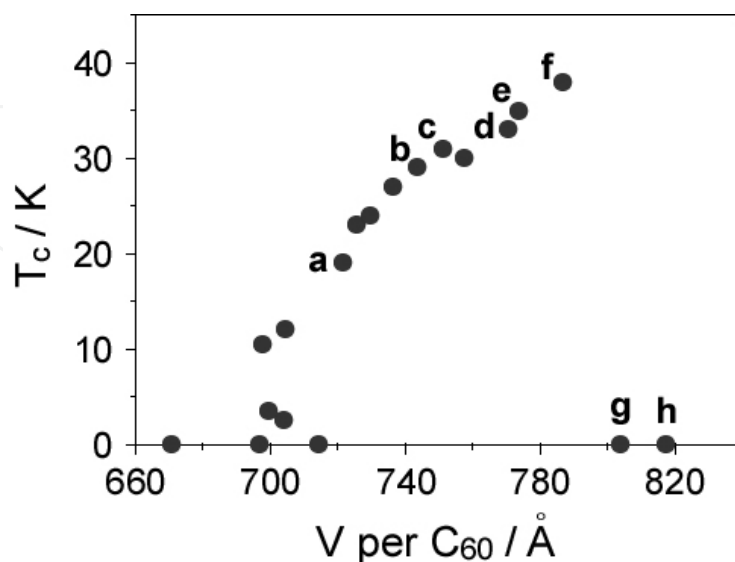

Figure 10. T_c as a function of volume occupied per C_{60}^{3-} in cubic M_3C_{60} (M: alkali metal). **a**: K_3C_{60}, **b**: Rb_3C_{60}, **c**: Rb_2CsC_{60}, **d**: $RbCs_2C_{60}$, **e**: fcc Cs_3C_{60} at 0.7 GPa, **f**: A15 Cs_3C_{60} at 0.7 GPa, **g**: fcc Cs_3C_{60} at AP, **h**: A15 Cs_3C_{60} at AP.

In 2008, A15 or body-centered cubic (bcc) Cs_3C_{60} phase, which shows the bulk superconductivity under an applied hydrostatic pressure, was obtained together with a small amount of by-products of body-centered orthorhombic (bco) and fcc phases, by a solution process in liquid methylamine [181]. Interestingly, the lattice contraction with respect to pressure results in the increase in T_c up to around 0.7 GPa, above which T_c gradually decreases. The trend in the initial pressure range is not explicable within the simple BCS theory. At AP, on the other hand, the A15 Cs_3C_{60} shows an AF ordering below 46 K, verified by means of ^{133}Cs NMR and μSR [182]. Very recently, it has been found that the fcc phase also shows an AF ordering at 2.2 K at AP and superconducting transition at 35 K under an applied hydrostatic pressure of about 0.7 GPa [183]. We note that T_c of the both phases follows the universal relationship for M_3C_{60} superconductors in the vicinity of the Mott boundary, as seen in Fig. 10. So far about 40 superconductors were prepared with the highest T_c of 33 K ($RbCs_2C_{60}$) at AP and 38 K (A15 Cs_3C_{60}) under pressure (0.7 GPa).

4. Polyaromatic hydrocarbon superconductors

Doping of alkali metals in picene (Scheme 8), that has a wider band gap (3.3 eV) than 1.8 eV for pentacene, introduced superconductivity [184]. The bulk superconducting phase was observed below 7 K and 18 K for K_3picene, and 7 K for Rb_3picene, which are comparable to that of K_3C_{60} ($T_c = 19$ K). Since the energy difference between LUMO and LUMO+1 is very small (< 0.1 eV), the three electrons reside in the almost two-fold degenerate LUMO.

Considering the fact that $Ca_{1.5}$picene also shows a superconducting phase below 7 K [185], three-fold charge transfer from dopants to one picene molecule would be responsible for emergence of the superconductivity. At present, although the crystal structures of the doped compounds are unclear, the refined lattice parameters are indicative of the deformation of the herringbone structure of pristine picene and the intercalation of dopants within the two-dimensional picene layers. After the discovery of the picene-based superconductors, several superconductors have been found for alkali metal (T_c = 7 K) [186] and alkaline-earth metal (T_c ~ 5.5 K) [187] doped phenanthrene, potassium-doped 1,2:8,9-dibenzopentacene (T_c = 33 K; partially decomposed) [188], and potassium-doped coronene (T_c < 15 K) [185]. Among them, phenanthrene-based superconductors shows an enhancement of T_c with increasing pressure, which is indicative of the non-BCS behavior.

phenanthrene   picene

1,2:8,9-dibenzopentacene   coronene
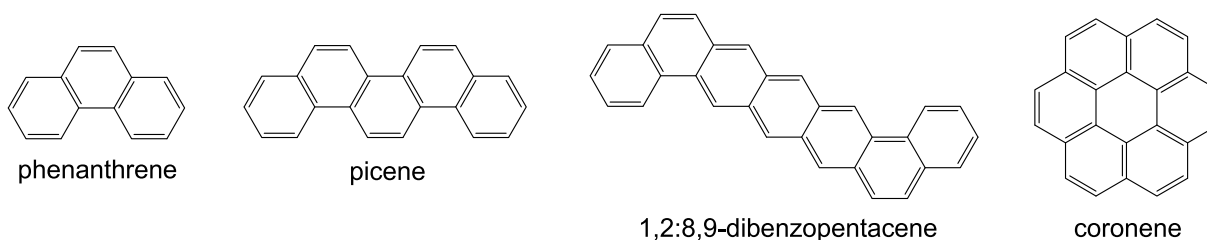
Scheme 8.

Contrary to the electron-doped system above described, it has been found that a cation radical salt (perylene)$_2$Au(mnt)$_2$, in which each perylene has an average charge of +0.5 and form segregated columns, show a superconductivity with T_c = 0.3 K when the hydrostatic pressure above 0.5 GPa was applied to suppress CDW phase [189]. So far 8 aromatic hydrocarbon superconductors were prepared with the highest T_c of 33 K at AP.

5. Carbon nanotubes, graphite, and diamond superconductors

In 2001, first superconducting carbon nanotubes were discovered for ropes of single-walled carbon nanotubes (SWNTs) with diameters of the order of 1.4 nm (T_c = 0.4 K) [190], and immediately after that SWNT with diameters of 0.4 nm embedded in a zeolite matrix (T_c = 15 K) [191,192]. The drop in magnetic susceptibility is more gradual than expected for three-dimensional superconductors, and superconducting gap estimated from the I-V plot shows the temperature dependency characteristic of one-dimensional fluctuations. It is apparent that the isolation of carbon nanotubes from each other is responsible for the realization of the almost ideal one-dimensional system. Multi-walled carbon nanotubes (MWNTs) also show the superconductivity; namely, MWNT with diameters of 10–17 nm that were grown in nanopores of alumina templates was found to show superconductivity with T_c = 12 K [193]. We note that this superconducting system is classified into single component superconductors, contrary to the C_{60} and graphite (*vide infra*) based superconductors.

Graphite has a layered structure composed of infinite benzene-fused π-planes (graphenes) with sp^2 character. First-stage alkali metal doped graphite intercalation compounds (GICs)

were known to superconduct with T_c = 0.15 K for KC$_8$ [194]. In 1980s and 1990s, further efforts were poured to synthesize GICs with higher T_c, such as LiC$_2$ with T_c = 1.9 K [195]. In 2005, these efforts culminated in the discovery of CaC$_6$ with T_c as high as 11.5 K at AP [196], which goes up to 15.1 K under pressures up to 7.5 GPa [197]. In other alkaline-earth metal doped GICs, the superconducting phase was observed below 1.65 K for SrC$_6$ and 6.5 K for YbC$_6$ [198]. The apparent reduction of T_c strongly suggests that the interlayer states of graphite have an impact on the electronic state of GIC, which was supported by theoretical calculations [199]. The conventional phonon mechanism in the framework of conventional BCS theory is generally accepted, due mainly to the observation of the Ca isotope effect with its exponent α = 0.5 [200].

A typical sp^3 covalent system, diamond, is an electrical insulator with a wide band gap of 5.5 eV, and is well known for its hardness as well as its unique electronic and thermal properties. Superconductivity in diamond was achieved through heavy p-type doping by boron in 2004 (T_c = 4 K), which was performed under high pressure (8–9 GPa) and high temperatures (2500–2800 K) [201]. Enhanced T_c in homoepitaxial CVD films has been achieved as high as 11 K [202]. Doped boron introduces an acceptor level with a hole binding energy of 0.37 eV and results in a metallic state above a critical boron concentration in the range of a few atoms per thousand. The T_c varies between 1 and 10 K with the doping level [203]. Superconducting gap estimated from STM [204] and isotopic substitution of boron and carbon [205] follow the BCS picture, as MgB$_2$ (T_c = 39 K).

Accordingly, all of the carbon polymorphs, namely zero-dimensional C$_{60}$ (sp^2/sp^3 character), one-dimensional carbon nanotube (sp^2 character), two-dimensional graphite (sp^2 character), and three-dimensional diamond (sp^3 character) could provide superconductors, despite their covalent character being different. The superconductors with sp^2/sp^3 or sp^2 carbons were realized either in themselves or by doping of metal atoms, while those with sp^3 carbons were realized by substitution of boron for carbon.

6. Single component superconductors

Since the discovery of the first metallic CT solid, TTF•TCNQ, in 1973 [8], much attention for organic (super)conductors has been devoted to plural component CT solids. Besides numerous studies on multi-component CT solids, several single-component organic conductors have been developed. Even though pentacene is known to be the first organic metal (semimetal) showing a decrease of resistivity down to ca. 200 K at 21.3 GPa [206], no superconductivity was reported so far on the solids composed of aromatic hydrocarbon solely. Electric conductivity increases by the enhancement of intermolecular interactions by appropriate use of hetero-atomic contacts. There are two single-component superconductors under extremely high pressure, p-iodanil (σ_{RT} = 1 $\times$ 10^{-12} S cm^{-1} at AP, σ_{RT} = 2 $\times$ 10 S cm^{-1} at 25 GPa, and superconductor at T_c ~ 2 K at 52 GPa) [207,208] and hexaiodobenzene (T_c = 0.6–0.7 K at around 33 GPa and ca. 2.3 K at 58 GPa) [209]. Both have peripheral chalcogen atoms, iodine, which may cause the increased electronic dimensionality of the solid under pressure owing to intermolecular iodine···iodine contacts.

p-iodanil   hexaiodobenzene
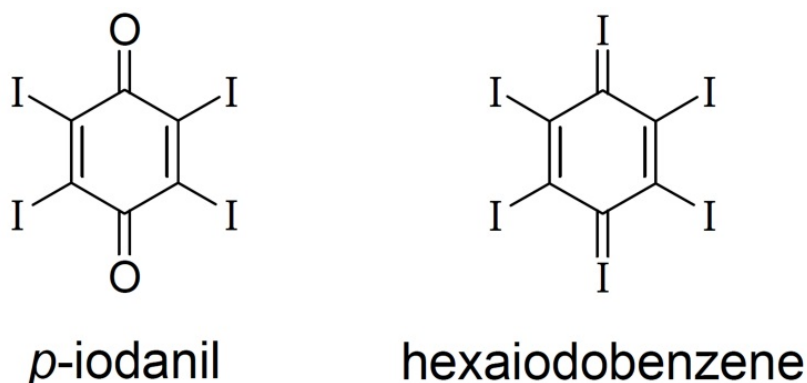
Scheme 9.

Abbreviations

AF: antiferromagnetic
AMRO: angular dependent magnetoresistance oscillation
AP: ambient pressure
BCS: Bardeen-Cooper-Schrieffer
CDW: charge density wave
CT: charge transfer
$D(\varepsilon_F)$: density of states at Fermi level (ε_F) per spin
dHvA: de Haas-van Alphen
FISDW: field induced spin-density-wave
GIC: graphite intercalation compound
H_{c2}: upper critical magnetic field
H_{Pauli}: Pauli limited magnetic field
LUMO: lowest unoccupied molecular orbital
MI: metal-insulator
MWNT: multi-walled carbon nanotubes
OD: order-disorder
P_c: critical pressure for superconductivity
SdH: Shubnikov-de Haas
SDW: spin density wave
STM: scanning tunneling microscope
SWNT: single-walled carbon nanotubes
t: transfer integral
T_c: critical temperature for superconductivity
T_N: Néel temperature (temperature for AF order)
U (U_{eff}): on-site Coulomb repulsion energy (effective U)
W: band width
Θ: Debye temperature

Author details

Gunzi Saito and Yukihiro Yoshida

Faculty of Agriculture, Meijo University, Shiogamaguchi 1-501 Tempaku-ku, Nagoya, Japan

7. References

[1]   Little W A (1964) Phys. Rev. A134: 1416-1424.

[2]   Greene R L, Street G B, Suter L J (1975) Phys. Rev. Lett. 34: 577-579.

[3]   Kawamura H, Shirotani I, Tachikawa K (1984) Solid State Commun. 49: 879-881.

[4]   Lee K, Cho S, Park S H, Heeger A J, Lee C-W, Lee S-H (2006) Nature 441: 65-68.

[5]   As a review see for example, Prassides K (2000) In: Andreoni W, editor. The Physics of Fullerene-Based and Fullerene-Related Materials. Boston: Kluwer Academic Publishers. pp. 175-202.

[6]   Akamatu H, Inokuchi H, Matsunaga Y (1954) Nature 173: 168-169.

[7]   As a review see for example, Hertler W R, Mahler W, Melby L R, Miller J S, Putscher R E, Webster O W (1989) Mol. Cryst. Liq. Cryst. 171: 205-216.

[8]   Ferraris J, Cowan D O, Walatka V, Perlstein J H (1973) J. Am. Chem. Soc. 95: 948-949.

[9]   Jerome D, Mazaud A, Ribault M, Bechgaard K (1980) J. Phys. Lett. 41: L95-L98.

[10] Lee I J, Naughton M J, Tanner G M, Chaikin P M (1997) Phys. Rev. Lett. 78: 3555-3558.

[11] Wudl F, Aharon-Shalom E, Nalewajek D, Waszeczak J V, Walsh Jr. W M, Rupp Jr. L W, Chaikin P M, Lacoe R, Burns M, Poehler T O, Williams J M, Beno M A, J. Chem. Phys. (1982) 76: 5497-5501.

[12] Sakata M, Yoshida Y, Maesato M, Saito G, Matsumoto K, Hagiwara R (2006) Mol. Cryst. Liq. Cryst. 452: 99-108.

[13] Jerome D, Schulz H J (1982) Adv. Phys. 31: 299-490.

[14] Jerome D (2004) Chem. Rev. 104: 5565-5591.

[15] Horiuchi S, Yamochi H, Saito G, Sakaguchi K, Kusunoki M (1996) J. Am. Chem. Soc. 118: 8604-8622.

[16] Saito G, Yoshida Y (2007) Bull. Chem. Soc. Jpn. 80: 1-137 and references cited therein.

[17] Ishiguro T, Yamaji K, Saito G (1998) Organic Superconductors, 2nd ed.: Springer-Verlag, Berlin.

[18] Williams J M, Ferraro J R, Thorn R J, Carlson K D, Geiser U, Wang H H, Kini A M, Whangbo M -H (1992) Organic Superconductors (Including Fullerenes): Prentice Hall, Englewood Cliffs, NJ.

[19] Wosnitza J (1996) Fermi Surfaces of Low-Dimensional Organic Metals and Superconductors: Springer-Verlag, Berlin.

[20] Singleton J (2000) Rep. Prog. Phys. 63: 1111-1207.

[21] Chem. Rev. (2004) 104, No. 11, Special Issue on Molecular Conductors.

[22] Balicas L, Behnia K, Kang W, Canadell E, Auban-Senzier P, Jerome D, Ribault M, Fabre J M (1994) J. Phys. I (France) 4: 1539-1549.

[23] Adachi T, Ojima E, Kato K, Kobayashi H, Miyazaki T, Tokumoto M, Kobayashi A (2000) J. Am. Chem. Soc. 122: 3238-3239.

[24] Auban-Senzier P, Pasquier C, Jerome D, Carcel C, Fabre J M (2003) Synth. Met. 133-134: 11-14.

[25] Itoi M, Araki C, Hedo M, Uwatoko Y, Nakamura T (2008) J. Phys. Soc. Jpn. 77: 023701/1-4.

[26] Takigawa M, Yasuoka H, Saito G (1987) J. Phys. Soc. Jpn. 56: 873-876.

[27] Hasegawa Y, Fukuyama H (1987) J. Phys. Soc. Jpn. 56: 877-880.

[28] Belin S, Behnia K (1997) Phys. Rev. Lett. 79: 2125-2128.

[29] Jerome D (1991) Science 252: 1509-1514. A more detail diagram was then proposed; Dumm M, Loidl A, Fravel B W, Starkey K P, Montgomery L K, Dressel M (2000) Phys. Rev. B61: 511-521.

[30] Beno M A, Wang H H, Kini A M, Carlson K D, Geiser U, Kwok W K, Thompson J E, Williams J M, Ren J, Whangbo M -H (1990) Inorg. Chem. 29: 1599-1601.

[31] Kahlich S, Schweitzer D, Heinen I, Lan S E, Nuber B, Keller H J, Winzer K, Helberg H W (1991) Solid State Commun. 80: 191-195.

[32] Saito G, Enoki T, Toriumi K, Inokuchi H (1982) Solid State Commun. 42: 557-560.

[33] Leung P C W, Emge T J, Beno M A, Wang H H, Williams J M, Patrick V, Coppens P (1985) J. Am. Chem. Soc. 107: 6184-6191.

[34] Saito G, Otsuka A, Zakhidov A A (1996) Mol. Cryst. Liq. Cryst. 284: 3-14.

[35] Baram O, Buravov L I, Degtyarev L S, Kozlov M E, Laukhin V N, Laukhina E E, Onishchenko V G, Pokhodnya K I, Sheinkman M K, Shibaeva R P, Yagubskii E B (1986) JETP Lett. 44: 376-378.

[36] Schweitzer D, Bele P, Brunner H, Gogu E, Haeberlen U, Hennig I, Klutz I, Sweitlik R, Keller H J (1987) Z. Phys. B 67: 489-495.

[37] Yoshimura M, Shigekawa H, Yamochi H, Saito G, Kawazu A (1991) Phys. Rev. B44: 1970-1972.

[38] Yoshimura M, Shigekawa H, Nejoh H, Saito G, Saito Y, Kawazu A (1991) Phys. Rev. B43: 13590-13593.

[39] Yoshimura M, Ara N, Kageshima M, Shiota R, Kawazu A, Shigekawa H, Saito Y, Oshima M, Mori H, Yamochi H, Saito G (1991) Surf. Sci. 242: 18-22.

[40] Yamochi H, Komatsu T, Matsukawa N, Saito G, Mori T, Kusunoki K, Sakaguchi K (1993) J. Am. Chem. Soc. 115: 11319-11327.

[41] Kobayashi A, Kato R, Kobayashi H, Moriyama S, Nishio Y, Kajita K, Sasaki W (1987) Chem. Lett. 459-462.

[42] Yagubskii E B, Shchegolev I F, Laukhin V N, Kononovich P A, Karstovnik M V, Zvarykina A V, Buravov L I (1984) JETP Lett. 39: 12-15.

[43] Shibaeva R P, Kaminskii V F, Yagubskii E B (1985) Mol. Cryst. Liq. Cryst. 119: 361-373.

[44] Kagoshima S, Mori H, Nogami Y, Kinoshita N, Anzai H, Tokumoto M, Saito G (1990) In: Saito G, Kagoshima S, editors. The Physics and Chemistry of Organic Superconductors: Springer-Verlag, Berlin, pp. 126-129.

[45] Laukhin V N, Kostyuchenko E E, Sushko Yu V, Shchegolev I F, Yagubskii E B (1985) Pis'ma Zh. Eksp. Teor. Fiz. 41: 68-70.

[46] Murata K, Tokumoto M, Anzai H, Bando H, Saito G, Kajimura K, Ishiguro T (1985) J. Phys. Soc. Jpn. 54: 1236-1239.

[47] Schirber J E, Azevedo L J, Kwak J F, Venturini E L, Leung P C W, Beno M A, Wang H H, Williams J M (1986) Phys. Rev. B33: 1987-1989.

[48] Wang H H, Nunez L, Carlson G W, Williams J M, Azevedo J L, Kwak J F, Schirber J E (1985) Inorg. Chem. 24: 2465-2466.

[49] Komatsu T, Nakamura T, Matsukawa N, Yamochi H, Saito G (1991) Solid State Commun. 80: 843-847.

[50] Fig.54 in Ref. 16.

[51] Urayama H, Yamochi H, Saito G, Nozawa K, Sugano T, Kinoshita M, Sato S, Oshima K, Kawamoto A, Tanaka J (1988) Chem. Lett. 55-58.

[52] Urayama H, Yamochi H, Saito G, Sato S, Kawamoto A, Tanaka J, Mori T, Maruyama Y, Inokuchi H (1988) Chem. Lett. 463-466.

[53] Oshima K, Mori T, Inokuchi H, Urayama H, Yamochi H, Saito G (1988) Phys. Rev. B38: 938-941.

[54] Fig. 53 in Ref. 16.

[55] Kini M, Geiser U, Wang H H, Carlson K D, Williams J M, Kwok W K, Vandervoort K G, Thompson J E, Stupka D L, Jung D, Wangbo M -H (1990) Inorg. Chem. 29: 2555-2557.

[56] Komatsu T, Matsukawa N, Nakamura T, Yamochi H, Saito G (1992) Phosphorus, Sulfur Silicon Relat. Elem. 67: 295-300, and Section 3-5-4-2 in Ref. 16.

[57] Williams J M, Kini A M, Wang H H, Carlson K D, Geiser U, Montgomery L K, Pyrka G J, Watkins D M, Kommers J M, Boryschuk S J, Crouch A V, Kwok W K, Schirber J E, Overmyer D L, Jung D, Whangbo M -H (1990) Inorg. Chem. 29: 3272-3274.

[58] Schirber J E, Overmyer D L, Carlson K D, Williams J M, Kini A M, Wang H H, Charlier H A, Love B J, Watkins D M, Yaconi G A (1991) Phys. Rev. B44: 4666-4669.

[59] Welp U, Fleshler S, Kwok W K, Crabtree G W, Carlson K D, Wang H H, Geiser U, Williams J M, Hitsman V M (1992) Phys. Rev. Lett. 69: 840-843. This paper mistakenly described that the AF transition occurred at 45 K and weak ferromagnetic transition at 23 K. The magnetic susceptibility measurements could not identify the transition either AF or SDW.

[60] Miyagawa K, Kawamoto K, Nakazawa Y, Kanoda K (1995) Phys. Rev. Lett. 75: 1174-1177.

[61] Geiser U, Wang H H, Carlson K D, Williams J M, Charlier Jr. H A, Heindl J E, Yaconi G A, Love B H, Lathrop M W, Schirber J E, Overmyer D L, Ren J, Whangbo M -H (1991) Inorg. Chem. 30: 2586-2588.

[62] Shimizu Y, Maesato M, Saito G, Drozdova O, Ouahab L (2003) Synth. Met. 133-134: 225-226.

[63] Shimizu Y, Miyagawa K, Kanoda K, Maesato M, Saito G (2003) Phys. Rev. Lett. 91: 107001/1-4.

[64] Pratt F L, Baker P J, Blundell S J, Lancaster T, Ohira-Kawamura S, Baines C, Shimizu Y, Kanoda K, Watanabe I, Saito G (2011) Nature 471: 612-616.

[65] Shimizu Y, Maesato M, Saito G (2011) J. Phys. Soc. Jpn. 80: 074702/1-7.

[66] Iwasa Y, Mizuhashi K, Koda T, Tokura Y, Saito G (1994) Phys. Rev. B49: 3580-3583.

[67] Yoneyama N, Miyazaki A, Enoki T, Saito G (1999) Bull. Chem. Soc. Jpn. 72: 639-651.

[68] Taniguchi H, Miyashita M, Uchiyama K, Satoh K, Mori N, Okamoto H, Miyagawa K, Kanoda K, Hedo M, Uwatoko Y (2003) J. Phys. Soc. Jpn. 72: 468-471.

[69] Uchiyama K, Miyashita M, Taniguchi H, Satoh K, Mori N, Miyagawa K, Kanoda K, Hedo M, Uwatoko Y (2004) J. Phys. IV 114: 387-389.

[70] Appendix (pp. 455-458) in Ref. 17.

[71] Sasaki T, Sato H, Toyota N (1990) Solid State Commun. 76: 507-510.

[72] Ito H, Watanabe M, Nogami Y, Ishiguro T, Komatsu T, Saito G, Hosoito N (1991) J. Phys. Soc. Jpn. 60: 3230-3233.

[73] Sushko Y V, Ito H, Ishiguro T, Horiuchi S, Saito G (1993) J. Phys. Soc. Jpn. 62: 3372-3375.

[74] Ito H, Ishiguro T, Kubota M, Saito G (1996) J. Phys. Soc. Jpn. 65: 2987-2993.

[75] Kubota M, Saito G, Ito H, Ishiguro T, Kojima N (1996) Mol. Cryst. Liq. Cryst. 284: 367-377.

[76] Ito H, Ishiguro T, Kondo T, Saito G (2000) J. Phys. Soc. Jpn. 69: 290-291.

[77] Posselt H, Muller H, Andres K, Saito G (1994) Phys. Rev. B49: 15849-15852.

[78] Lefebvre S, Wzietek P, Brown S, Bourbonnais C, Jérome D, Mézière C, Fourmigué M, Batial P (2000) Phys. Rev. Lett. 85: 5420-5423.

[79] Tanatar M A, Ishiguro T, Kagoshima S, Kushch N D, Yagubskii E B (2002) Phys. Rev. B65: 064516/1-5.

[80] Kanoda K (2006) J. Phys. Soc. Jpn. 75: 051007/1-16.

[81] Schulueter J A, Wiehl L, Park H, de Souza M, Lang M, Koo H -J, Whangbo M -H (2010) J. Am. Chem. Soc. 132: 16308-16310.

[82] Kawamoto T, Mori T, Nakao A, Murakami Y, Schlueter J A (2012) J. Phys. Soc. Jpn. 81: 023705/1-4.

[83] Pereiro J, Petrovic A, Panagopoulos C, Božović I (2011) Phys. Express 1: 208-241.

[84] Gariglio S, Triscone J -M (2011) C. R. Phys. 12: 591-599.

[85] Kartsovnik M V, Logvenov G Yu, Ito H, Ishiguro T, Saito G (1995) Phys. Rev. B52: R15715- R15718.

[86] Weiss H, Kartsovnik M V, Biberacher W, Steep E, Balthes E, Jansen A G M, Andres K, Kushch N D (1999) Phys. Rev. B59: 12370-12378.

[87] Kartsovnik M V, Biberacher W, Andres K, Kushch N D (1995) JETP Lett. 62: 905-909.

[88] Oshima K, Urayama H, Yamochi H, Saito G (1988) J. Phys. Soc. Jpn. 57: 730-733.

[89] Nam M -S, Symington J A, Singleton J, Blundell S J, Ardavan A, Perenboom J A A J, Kurmoo M, Day P (1999) J. Phys.: Condens. Matter 11: L477-484.

[90] Arai T, Ichimura K, Nomura K (2001) Phys. Rev. B63: 104518/1-5.

[91] Izawa K, Yamaguchi H, Sasaki T, Matsuda Y (2002) Phys. Rev. Lett. 88: 27002/1-4.

[92] Ichimura K, Takami M, Nomura K (2008) J. Phys. Soc. Jpn. 77: 114707/1-6.

[93] Malone L, Taylor O J, Schlueter J A, Carrington A (2010) Phys. Rev. B82: 014522/1-5.

[94] Toyota N (1996) In: Physical Phenomena at High Magnetic Fields-II. World Sci., pp. 282-293.

[95] McKenzie R H (1998) Comments Condens. Matter Phys. 18: 309-337.

[96] Kino H, Fukuyama H (1995) J. Phys. Soc. Jpn. 64: 2726-2729.

[97] Wannier G H (1950) Phys. Rev. 79: 357-364.

[98] Anderson P W (1973) Mater. Res. Bull. 8: 153-164.

[99] Balents L (2010) Nature 464: 199-208.

[100] Norman M R (2011) Science 332: 196-200.

[101] Furukawa Y, Sumida Y, Kumagai K, Borsa F, Nojiri H, Shimizu Y, Amitsuka H, Tenya K, Kögerler P, Cronin L, (2011) J. Phys.: Conf. Ser. 320: 012047/1-6.

[102] Seeber G, Kögerler P, Kariuki B M, Cronin L (2004) Chem. Commun. 1580-1581.

[103] Itou T, Oyamada A, Maegawa S, Tamura M, Kato R (2007) J. Phys.: Condens. Matter 19: 145247/1-5.

[104] Shores M P, Nytko E A, Bartlett B M, Nocera D G (2005) J. Am. Chem. Soc. 127: 13462-13463.

[105] Mendels P, Bert F (2010) J. Phys. Soc. Jpn. 79: 011001/1-10.

[106] Okamoto Y, Nohara M, Aruga-Katori H, Takagi H (2007) Phys. Rev. Lett. 99: 137207/1-4.

[107] Okamoto Y, Yoshida H, Hiroi Z (2009) J. Phys. Soc. Jpn. 78: 033701/1-4.

[108] Colman R H, Bert F, Boldrin D, Hiller A D, Manuel P, Mendels P, Wills A S (2011) Phys. Rev. B83: 180416/1-4.

[109] Coldea R, Tennante D A, Tylczynski Z (2003) Phys. Rev. B68: 134424/1-16.

[110] Nakatsuji S, Nambu Y, Tonomura H, Sakai O, Broholm C, Tsunetsugu H, Qiu Y, Maeno Y (2005) Science 309: 1697-1700.

[111] Olariu A, Mendels P, Bert F, Ueland B G, Schiffer P, Berger R F, Cava R J (2006) Phys. Rev. Lett. 97: 167203/1-4.

[112] Kimmel A, Mucksch M, Tsurkan V, Koza M M, Mutka H, Loidl A (2005) Phys. Rev. Lett. 94: 237402/1-4.

[113] Yoshida H, Okamoto Y, Tayama T, Sakakibara T, Tikunaga M, Matsuo A, Narumi Y, Kindo K, Yoshida M, Takigawa M, Hiroi Z (2009) J. Phys. Soc. Jpn. 78: 043704/1-4.

[114] Iwasa Y, Takenobu T (2003) J. Phys.: Condens. Matter 15: R495-R519.

[115] Chu C W (2009) Nat. Phys. 5: 787-789.

[116] Maesato M, Shimizu Y, Ishikawa T, Saito G, Miyagawa K, Kanoda K (2004) J. Phys. IV 114: 227-232.

[117] Tajima N, Ebina-Tajima A, Tamura M, Nishio Y, Kajita K (2002) J. Phys. Soc. Jpn. 71: 1832-1835.

[118] Shibaeva R P, Kaminskii V F, Yagubskii E B (1985) Mol. Cryst. Liq. Cryst. 119: 361-373.

[119] Kobayashi H, Kato R, Kobayashi A, Nishio Y, Kajita K, Sasaki W (1986) Chem. Lett. 789-792.

[120] Ito H, Ishihara T, Niwa M, Suzuki T, Onari S, Tanaka Y, Yamada J, Yamochi H, Saito G (2010) Physica B 405: S262-264.

[121] Emge T J, Leung P C W, Beno M A, Schultz A J, Wang H H, Sowa L M, Williams J M (1984) Phys. Rev. B30: 6780-6782.

[122] Bender K, Dietz K, Endres H, Helberg H V, Hennig I, Keller H J, Schafer H V, Schweitzer D (1984) Mol. Cryst. Liq. Cryst. 107: 45-53.

[123] Takano Y, Hiraki K, Yamamoto H M, Nakamura T, Takahashi T (2001) J. Phys. Chem. Solids 62: 393-395.

[124] Tajima N, Sugawara S, Tamura M, Nishio Y, Kajita K (2006) J. Phys. Soc. Jpn. 75: 051010/1-10.

[125] Katayama S, Kobayashi A, Suzumura Y (2006) J. Phys. Soc. Jpn. 75: 054705/1-6.

[126] Kondo R, Kagoshima S, Maesato M (2003) Phys. Rev. B67: 134519/1-6.

[127] Kobayashi H, Kato R, Kobayashi A, Nishio Y, Kajita K, Sasaki W (1986) 789-792: 833-836.

[128] Mori H, Tanaka S, Mori T (1998) Phys. Rev. B57: 12023-12029.

[129] Salameh B, Nothardt A, Balthes E, Schmidt W, Schweitzer D, Strempfer J, Hinrichsen B, Jansen M, Maude D K (2007) Phys. Rev. B75: 054509/1-13.

[130] Tanaka H, Ojima E, Fujiwara H, Nakazawa Y, Kobayashi H, Kobayashi A (2000) J. Mater. Chem. 10: 245-247.

[131] Kobayashi H, Tomita H, Naito T, Kobayashi A, Sakai F, Watanabe T, Cassoux P (1996) J. Am. Chem. Soc. 118: 368-377.

[132] Uji S, Shinagawa H, Terashima T, Yakabe T, Terai Y, Tokumoto M, Kobayashi A, Tanaka H, Kobayashi H (2001) Nature 410: 908-910.

[133] Matsui H, Tsuchiya H, Suzuki T, Negishi E, Toyota N (2003) Phys. Rev. B68: 155105/1-10.

[134] Toyota N, Abe Y, Matsui H, Negishi E, Ishizaki Y, Tsuchiya H, Uozaki H, Endo S (2002) Phys. Rev. B66: 033201/1-4.

[135] Kobayashi H, Sato A, Arai E, Akutsu H, Kobayashi A, Cassoux P (1997) J. Am. Chem. Soc. 119: 12392-12393.

[136] Fujiwara E, Fujiwara H, Kobayashi H, Otsuka T, Kobayashi A (2002) Adv. Mater. 14: 1376-1379.

[137] Meul H W, Rossel C, Decroux M, Fischer Ø, Remenyi G, Briggs A (1984) Phys. Rev. Lett. 53: 497-500.

[138] Lin C L, Teter J, Crow J E, Mihalisin T, Brooks J, Abou-Aly A I, Stewart G R (1985) Phys. Rev. Lett. 54: 2541-2544.

[139] Clark K, Hassanien A, Khan S, Braun K -F, Tanaka H, Hla S -W (2010) Nature Nanotech. 5: 261-265.

[140] Sakata J, Sato H, Miyazaki A, Enoki T, Okano Y, Kato R (1998) Solid State Commun. 108: 377-381.

[141] Yamada J, Watanabe M, Akutsu H, Nakatsuji S, Nishikawa H, Ikemoto I, Kikuchi K (2001) J. Am. Chem. Soc. 123: 4174-4180.

[142] Ito H, Ishihara T, Tanaka H, Kuroda S, Suzuki T, Onari S, Tanaka Y, Yamada J, Kikuchi K (2008) Phys. Rev. B78: 172506/1-4.

[143] Shimojo Y, Ishiguro T, Toita T, Yamada J (2002) J. Phys. Soc. Jpn. 71: 717-720.

[144] Nomura K, Muraoka R, Matsunaga N, Ichimura K, Yamada J (2009) Physica B 404: 562-564.

[145] Okano Y, Iso M, Kashimura Y, Yamaura J, Kato R (1999) Synth. Met. 102: 1703-1704.

[146] Zambounis J S, Mayer C W, Hauenstein K, Hilti B, Hofherr W, Pfeiffer J, Buerkle M, Rihs G (1992) Adv. Mater. 4: 33-35.

[147] Kimura S, Maejima T, Suzuki H, Chiba R, Mori H, Kawamoto T, Mori T, Moriyama H, Nishio Y, Kajita K (2004) Chem. Commun. 2454-2455.

[148] Kimura S, Suzuki H, Maejima T, Mori H, Yamaura J, Kakiuchi T, Sawa H, Moriyama H (2006) J. Am. Chem. Soc. 128: 1456-1457.

[149] Kikuchi K, Murata K, Honda Y, Namiki T, Saito K, Ishiguro T, Kobayashi K, Ikemoto I (1987) J. Phys. Soc. Jpn. 56: 3436-3439.

[150] Nishikawa H, Morimoto T, Kodama T, Ikemoto I, Kikuchi K, Yamada J, Yoshino H, Murata K (2002) J. Am. Chem. Soc. 124: 730-731.

[151] Kato R, Yamamoto K, Okano Y, Tajima H, Sawa H (1997) Chem. Commun. 947-948.

[152] Kato R, Aonuma S, Okano Y, Sawa H, Tamura M, Kinoshita M, Oshima K, Kobayashi A, Bun K, Kobayashi H (1993) Synth. Met. 61: 199-206.

[153] Imakubo T, Tajima N, Tamura M, Kato R, Nishio Y, Kajita K (2002) J. Mater. Chem. 12: 159-161.

[154] Lyubovskaya R N, Zhilyaeva E I, Torunova S A, Mousdis G A, Papavassiliou G C, Perenboom J A A J, Pesotskii S I, Lyubovskii R B (2004) J. Phys. IV 114: 463-466.

[155] Papavassiliou G C, Mousdis G A, Zambounis J S, Terzis A, Hountas A, Hilti B, Mayer C W, Pfeiffer J, Synth. Met. (1988) B27: 379-383.

[156] Takahashi T, Kobayashi Y, Nakamura T, Kanoda K, Hilti B, Zambounis J S (1994) Physica C235-240: 2461-24562.

[157] Takimiya K, Takamori A, Aso Y, Otsubo T, Kawamoto T, Mori T (2003) Chem. Mater. 15: 1225-1227.

[158] Kawamoto T, Mori T, Enomoto K, Koike T, Terashima T, Uji S, Takamori A, Takimiya K, Otsubo T (2006) Phys. Rev. B73: 024503/1-5.

[159] Takimiya K, Kodani M, Niihara N, Aso Y, Otsubo T, Bando Y, Kawamoto T, Mori T (2004) Chem. Mater. 16: 5120-5123.

[160] Takimiya K, Kataoka Y, Aso Y, Otsubo T, Fukuoka H, Yamanaka S (2001) Angew. Chem., Int. Ed. 40: 1122-1125.

[161] Kawamoto T, Mori T, Konoike T, Enomoto K, Terashima T, Uji S, Kitagawa H, Takimiya K, Otsubo T (2006) Phys. Rev. B73: 094513/1-8.

[162] Kawamoto T, Mori T, Terakura C, Terashima T, Uji S, Takimiya K, Aso Y, Otsubo T (2003) Phys. Rev. B67: 020508/1-4.

[163] Kawamoto T, Mori T, Terakura C, Terashima T, Uji S, Tajima H, Takimiya K, Aso Y, Otsubo T (2003) Eur. Phys. J. B 36: 161-167.

[164] Kodani M, Takamori A, Takimiya K, Aso Y, Otsubo T (2002) J. Solid State Chem. 168: 582-589.

[165] Misaki Y, Higuchi N, Fujiwara H, Yamabe T, Mori T, Mori H, Tanaka S (1995) Angew. Chem., Int. Ed. Engl. 34: 1222-1225.

[166] Shirahata T, Kibune M, Imakubo T (2006) Chem. Commun. 1592-1594.

[167] Shirahata T, Kibune M, Yoshino H, Imakubo T (2007) Chem. Eur. J. 13: 7619-7630.

[168] Hebard A F, Rosseinsky M J, Haddon R C, Murphy D W, Glarum S H, Palstra T T M, Ramirez A P, Kortan A R (1991) Nature 350: 600-601.

[169] Krätschmer W, Lamb L D, Fostiropoulos K, Huffman D R (1990) Nature 347: 354-358.

[170] Stephens P W, Mihaly L, Lee P L, Whetten R L, Huang S -M, Kaner R, Diederich F, Holczer K (1991) Nature 351: 632-634.

[171] Rosseinsky M J, Ramirez A P, Glarum S H, Murphy D W, Haddon R C, Hebard A F, Palstra T T M, Kortan A R, Zahurak S M, Makhija A V (1991) Phys. Rev. Lett. 66: 2830-2832.

[172] Tanigaki K, Ebbesen T W, Saito S, Mizuki J, Tsai J -S, Kubo Y, Kuroshima S (1991) Nature 352: 222-223.

[173] Fleming R M, Ramirez A P, Rosseinsky M J, Murphy D W, Haddon R C, Zahurak S M, Makhija A V (1991) Nature 352: 787-788.

[174] Sasaki S, Matsuda A, Chu C W (1994) J. Phys. Soc. Jpn. 63: 1670-1673.

[175] Kiefl R F, MacFarlane W A, Chow K H, Dunsiger S, Duty T L, Johnston T M S, Schneider J W, Sonier J, Brard L, Strongin R M, Fischer J E, Smith III A B (1993) Phys. Rev. Lett. 70: 3987-3990.

[176] Chen C -C, Lieber C M (1993) Science 259: 655-658.

[177] Takenobu T, Muro T, Iwasa Y, Mitani T (2000) Phys. Rev. Lett. 85: 381-384.

[178] Dahlke P, Denning M S, Henry P F, Rosseinsky M J (2000) J. Am. Chem. Soc. 122: 12352-12361.

[179] Yildirim T, Barbedette L, Fischer J E, Lin C L, Robert J, Petit P, Palstra T T M (1996) Phys. Rev. Lett. 77: 167-170.

[180] Kosaka M, Tanigaki K, Prassides K, Margadonna S, Lappas A, Brown C M, Fitch A N (1999) Phys. Rev. B59: R6628-R6630.

[181] Ganin A Y, Takabayashi Y, Khimyak Y Z, Margadonna S, Tamai A, Rosseinsky M J, Prassides K (2008) Nat. Mat. 7: 367-371.

[182] Takabayashi Y, Ganin A Y, Jeglič P, Arčon D, Takano T, Iwasa Y, Ohishi Y, Takata M, Takeshita N, Prassides K, Rosseinsky M J (2009) Science 323: 1585-1590.

[183] Ganin A Y, Takabayashi Y, Jeglič P, Arčon D, Potočnik A, Baker P J, Ohishi Y, McDonald M T, Tzirakis M D, McLennan A, Darling G R, Takata M, Rosseinsky M J, Prassides K (2010) Nature 466: 221-225.

[184] Mitsuhashi R, Suzuki Y, Yamanari Y, Mitamura H, Kambe T, Ikeda N, Okamoto H, Fujiwara A, Yamaji M, Kawasaki N, Maniwa Y, Kubozono Y (2010) Nature 464: 76-79.

[185] Kubozono Y, Mitamura H, Lee X, He X, Yamanari Y, Takahashi Y, Suzuki Y, Kaji Y, Eguchi R, Akaike K, Kambe T, Okamoto H, Fujiwara A, Kato T, Kosugi T, Aoki H (2011) Phys. Chem. Chem. Phys. 13: 16476-16493.

[186] Wang X F, Liu R H, Gui Z, Xie Y L, Yan Y J, Ying J J, Luo X G, Chen X H (2011) Nat. Commun. 2: 507-513.

[187] Wang X F, Yan Y J, Gui Z, Liu R H, Ying J J, Luo X G, Chen X H (2011) Phys. Rev. B84: 214523/1-4.

[188] Xue M, Cao T, Wang D, Wu Y, Yang H, Dong X, He J, Li F, Chen G F (2012) Sci. Rep. 2: 389/1–4.

[189] Graf D, Brooks J S, Almeida M, Dias J C, Uji S, Terashima T, Kimata M (2009) Europhys. Lett. 85: 27009/1-5.

[190] Kociak M, Kasumov A Yu, Guéron S, Reulet B, Khodos I I, Gorbatov Yu B, Volkov V T, Vaccarini L, Bouchiat H (2001) Phys. Rev. Lett. 86: 2416-2419.

[191] Tang Z K, Zhang L, Wang N, Zhang X X, Wen G H, Li G D, Wang J N, Chan C T, Sheng P (2001) Science 292: 2462-2465.

[192] Lortz R, Zhang Q, Shi W, Ye J T, Qiu C, Wang Z, He H, Sheng P, Qian T, Tang Z, Wang N, Zhang X, Wang J, Chan C T (2009) Proc. Natl. Acad. Sci. USA 106: 7299-7303.

[193] Takesue I, Haruyama J, Kobayashi N, Chiashi S, Maruyama S, Sugai T, Shinohara H (2006) Phys. Rev. Lett. 96: 057001/1-4.

[194] Hannay N B, Geballe T H, Matthias B T, Andres K, Schmidt P, MacNair D (1965) Phys. Rev. Lett. 14: 225-226.

[195] Belash I T, Bronnikov A D, Zharikov O V, Pal'nichenko A V (1989) Solid State Commun. 69: 921-923.

[196] Weller T E, Ellerby M, Saxena S S, Smith R P, Skipper N T (2005) Nat. Phys. 1: 39-41.

[197] Gauzzi A, Takashima S, Takeshita N, Terakura C, Takagi H, Emery N, Hérold C, Lagrange P, Loupias, G (2007) Phys. Rev. Lett. 98: 067002/1-4.

[198] Kim J S, Boeri L, O'Brien J R, Razavi F S, Kremer R K (2007) Phys. Rev. Lett. 99: 027001/1-4.

[199] Csányi G, Littlewood P B, Nevidomskyy A H, Pikard C J, Simons B D (2005) Nat. Phys. 1: 42-45.

[200] Hinks D G, Rosenmann D, Claus H, Bailey M S, Jorgensen J D (2007) Phys. Rev. B75: 014509/1-6.

[201] Ekimov E A, Sidorov V A, Bauer E D, Mel'nik N N, Curro N J, Thompson J D, Stishov S M (2004) Nature 428: 542-545.

[202] Takano Y, Takenouchi T, Ishii S, Ueda S, Okutsu T, Sakaguchi I, Umezawa H, Kawarada H, Tachiki M (2007) Diamond Relat. Mater. 16: 911-914.

[203] Bustarret E, Kačmarčik J, Marcenat C, Gheeraert E, Cytermann C, Marcus J, Klein T (2004) Phys. Rev. Lett. 93: 237005/1-4.

[204] Sacépé B, Chapelier C, Marcenat C, Kačmarčik J, Klein T, Bernard M, Bustarret E (2006) Phys. Rev. Lett. 96: 097006/1-4.

[205] Ekimov E A, Sidorov V A, Zoteev A V, Lebed J B, Thompson J D, Stishov S M (2008) Sci. Technol. Adv. Mater. 9: 044210/1-6.

[206] Aust R B, Bentley W H, Drickamer H G (1964) J. Chem. Phys. 41: 1856-1864.

[207] Yokota T, Takeshita N, Shimizu K, Amaya K, Onodera A, Shirotani I, Endo S (1996) Czech. J. Phys. 46: 817-818.

[208] Amaya K, Shimizu K, Takeshita N, Eremets M I, Kobayashi T C, Endo S (1998) J. Phys.: Condens. Matter 10: 11179-11190.

[209] Iwasaki E, Shimizu K, Amaya K, Nakayama A, Aoki K, Carlon R P (2011) Synth. Met. 120: 1003-1004.